DP-1550
Distribution Category: UC-25

# CORROSION OF HIGH Ni-Cr ALLOYS AND TYPE 304L STAINLESS STEEL IN $HNO_3$-HF

by

**R. S. ONDREJCIN**

and

**B. D. McLAUGHLIN**

Approved by

S. D. Harris, Research Manager

Publication Date: April 1980

DISCLAIMER

This book was prepared as an account of work sponsored by an agency of the United States Government. Neither the United States Government nor any agency thereof, nor any of their employees, makes any warranty, express or implied, or assumes any legal liability or responsibility for the accuracy, completeness, or usefulness of any information, apparatus, product, or process disclosed, or represents that its use would not infringe privately owned rights. Reference herein to any specific commercial product, process, or service by trade name, trademark, manufacturer, or otherwise, does not necessarily constitute or imply its endorsement, recommendation, or favoring by the United States Government or any agency thereof. The views and opinions of authors expressed herein do not necessarily state or reflect those of the United States Government or any agency thereof.

**E. I. du Pont de Nemours & Co.**
**Savannah River Laboratory**
**Aiken, SC 29808**

PREPARED FOR THE U. S. DEPARTMENT OF ENERGY UNDER CONTRACT DE-AC09-76SR00001

DISTRIBUTION OF THIS DOCUMENT IS UNLIMITED

## DISCLAIMER

**This report was prepared as an account of work sponsored by an agency of the United States Government. Neither the United States Government nor any agency Thereof, nor any of their employees, makes any warranty, express or implied, or assumes any legal liability or responsibility for the accuracy, completeness, or usefulness of any information, apparatus, product, or process disclosed, or represents that its use would not infringe privately owned rights. Reference herein to any specific commercial product, process, or service by trade name, trademark, manufacturer, or otherwise does not necessarily constitute or imply its endorsement, recommendation, or favoring by the United States Government or any agency thereof. The views and opinions of authors expressed herein do not necessarily state or reflect those of the United States Government or any agency thereof.**

**DISCLAIMER**

**Portions of this document may be illegible in electronic image products. Images are produced from the best available original document.**

## ABSTRACT

Nineteen alloys were evaluated as possible materials of construction for steam heating coils, the dissolver vessel, and the off-gas system of proposed facilities to process thorium and uranium fuels. Commercially available alloys were found that are satisfactory for all applications.

With thorium fuel, which requires $HNO_3$-HF for dissolution, the best alloy for service at 130°C when complexing agents for fluoride are used is Inconel® 690 (Huntington Alloys, Inc.); with no complexing agents at 130°C, Inconel® 671 is best. At 95°C, six other alloys tested would be adequate: Haynes® 25, (Cabot Corp.) Ferralium® (Cabot Corp.), Inconel® 625, Type 304L stainless steel, Incoloy® 825 (Huntington Alloys, Inc.), and Haynes® 20 (in order of decreasing preference); based on composition, six untested alloys would also be adequate. The ions most effective in reducing fluoride corrosion were the complexing agents $Zr^{4+}$ and $Th^{4+}$; $Al^{3+}$ was less effective.

With uranium fuel, modestly priced Type 304L stainless steel is adequate. Corrosion will be most severe in $HNO_3$-HF used occasionally for flushing and in solutions of $HNO_3$ and corrosion products (ferric and dichromate ions). HF corrosion can be minimized by complexing the fluoride ion and by passivation of the steel with strong nitric acid. Corrosion caused by corrosion products can be minimized by operating at lower temperatures.

## CONTENTS

## INTRODUCTION

The Savannah River Laboratory is developing programs for reprocessing irradiated thorium and uranium with minimum risk of nuclear weapons proliferation. This has required two separate, but similar programs.

The first development program is assessing the aqueous reprocessing of thorium reactor fuel. Processing of thorium and uranium fuel is similar. However, very little thorium has been used as nuclear fuel. Two major problems involve handling the small amount of $^{232-233}U$ that the irradiated thorium fuel contains and selecting materials of construction. The $^{232}U$ decays to $^{208}Tl$ with a 2.6-MeV gamma, which requires heavy shielding, especially if the uranium is to be fabricated into reactor fuel. The dissolution of $ThO_2$ requires $HNO_3$-HF, which is highly corrosive especially when hot.

Materials were evaluated for a $ThO_2$ dissolver in the 1960s[1-6] when thorium fuel was considered. These studies assumed that fluorides in acidic media would be used. Two literature summaries of the work were prepared, one by Allied Chemical at Idaho,[7] and one by Oak Ridge.[8] Although much of the information in these summaries is useful, many of the alloys tested were either experimental or are no longer manufactured. The two metals known to be resistant to $HNO_3$-HF, platinum and gold, are too expensive to be considered.

The second program is for irradiated uranium fuel from commercial power reactors. These fuels are dissolved, and the uranium is separated from the small amounts of plutonium and fission products by solvent extraction. The uranium and plutonium are purified, the offgases are treated, and the liquid nuclear waste is stored. This program is designed to close the back end of the nuclear fuel cycle.

This report summarizes an experimental program to identify suitable construction materials that are commercially available. For thorium reprocessing, the materials for the $ThO_2$ dissolver, steam heating coils, and off-gas system were considered because conditions are most corrosive. For uranium reprocessing, $HNO_3$ is the primary solvent. Occasionally HF may be added to the solvent to dissolve insolubles. The primary material of construction, Type 304L stainless steel, is attacked by HF. The precautions necessary to prevent excessive corrosion were evaluated.

## ALLOYS FOR USE WITH THORIUM FUEL

### Selection of Alloys for Corrosion Tests

Ten of nineteen candidate alloys were selected for corrosion tests. Compositions are listed in Table 1. Six others not tested because their compositions are similar are Inconel® 601 and 617, Hastelloy® X, Haynes® 188, and Types 309 and 310 stainless steel. The other three alloys were not tested because they are not readily available: Corronel® 230 (Henry Wiggins Co.), HAPO 20 (an experimental alloy made for Hanford by Battelle), and Blaw Knox NA 55 (not available in the wrought form).

High Ni-Cr alloys are the primary candidate materials for containing hot $HNO_3$-HF solutions. Type 304L stainless steel, a relatively low Ni-Cr alloy, was used as the baseline for corrosion measurements.

TABLE 1

Test Alloy Compositions, wt %

| *Alloy* | *Ni* | *Cr* | *Fe* | *Co* | *Mo* | *W* | *Cu* | *Others* |
|---|---|---|---|---|---|---|---|---|
| Inconel® 690 | 62 | 27 | 10 | - | - | - | - | - |
| Inconel® 625 | 61 | 27 | 4 | - | 9 | - | - | 3Nb + Ta |
| Inconel® 671* | 52 | 48 | - | - | - | - | - | - |
| Incoloy® 825 | 43 | 22 | 30 | 0 | 3 | 0 | 2 | 1Ti |
| Hastelloy® C-276** | 57 | 15 | 6 | 2 | 15 | 4 | - | - |
| Hastelloy® G | 44 | 22 | 19 | 2 | 7 | 1 | 2 | 2Nb + Ta, 1Mn |
| Haynes® 20 | 22 | 22 | 46 | 0 | 4 | 0 | 2 | 1Mn |
| Haynes® 25 | 10 | 20 | 2 | 51 | - | 15 | - | 2Mn |
| Ferralium® | 5 | 28 | 64 | - | 3 | - | 2 | 1Mn |
| Type 304L Stainless Steel | 8 | 19 | 71 | - | - | - | - | 2Mn |

* Powder metallurgy product.
**Trademark of Cabot Corporation.

## Electrochemical Corrosion Tests

Two electrochemical tests were evaluated for rapidly measuring corrosion rates of alloys. Both measure instantaneous rates (the rate at the time of measurement). The first method is linear polarization,[9] also known as the polarization-resistance method. The second method is the Corrosion Behavior Diagram developed by the International Nickel Company[10] for testing Inconel® and Incoloy® alloys. Linear polarization was found to be best for our tests.

### Linear Polarization Method

The linear polarization method is based on the Stern-Geary[9] equation:

$$I_{corr} = \frac{\beta_a \beta_c}{2.3 (\beta_a + \beta_c)} \frac{\Delta i}{\Delta E} \qquad (1)$$

where

$I_{corr}$ = corrosion current

$\beta_a$ = anodic Tafel slope

$\beta_c$ = cathodic Tafel slope

$\frac{\Delta i}{\Delta E}$ = slope of the linear polarization curve

The linear polarization curve is a plot of current versus potential with current being the independent variable. The slope of the curve is measured over the first 10 to 30 mV in either the anodic or cathodic direction. Small voltage increments are used to avoid perturbing the corroding system.

To apply the Stern-Geary equation, values for $\beta_a$ and $\beta_c$ must either be assumed or determined from a separate experimental semilogarithmic polarization curve. Assumed values are usually used because measurements are very time consuming. For ferrous alloys, 0.12 V/decade is usually assumed for both $\beta_a$ and $\beta_c$. In this case, Equation 1 becomes:

$$I_{corr} = 0.026 \, \Delta i/\Delta E \qquad (2)$$

When corrosion current is determined by either equation, the total amount of metal dissolved and, therefore, the extent of uniform penetration can be calculated from Faraday's Law. First, the electrochemical equivalent of the alloy (grams dissolved per coulomb of electrical flow) must be calculated. The outer shell electrons are assumed to be removed. Also, the electrochemical equivalent weight of the alloy is proportioned to the sum of the elemental weight fractions. For example, the electrochemical equivalent of Type 304L stainless steel is:

$$k_{304L} = 0.71\ k_{Fe} + 0.19\ k_{Cr} + 0.09\ k_{Ni}$$

$$\text{where } k = \frac{\text{gram atomic weight}}{(\text{Number of outer shell electrons})\ (96{,}500)}$$

and Fe is assumed to lose two electrons, Cr three, and Ni two. Faraday's Law, Equation 3, is then used to determine the total mass of metal dissolved (M):

$$M = kIt \qquad (3)$$

where k = electrochemical equivalent

I = corrosion current from Equation 2

t = time

The value of M is used with sample surface area and density to calculate the uniform penetration rate at the time of measurement.

Corrosion Behavior Diagram Method

In this method, $I_{corr}$ is determined graphically in a three-step procedure: (1) a very rapid potentiodynamic polarization curve (plot of voltage against current density) is run from low cathodic to high anodic currents to obtain a cathodic and an anodic scan; (2) a second scan is run in the reverse direction; and (3) the sample is allowed to stabilize at the open circuit potential and a third cathodic scan is run. Data from the third scan is expected to be between those of the first two cathodic scans. The linear portion of the second cathodic scan is extrapolated to the stabilized open circuit potential. $I_{corr}$ is the current at this point.

In the initial tests with Type 304L stainless steel in $HNO_3$-HF solutions, Corrosion Behavior Diagrams showed unusual characteristics not described in Reference 10. Although data could be extrapolated and values for $I_{corr}$ determined, the third cathodic scan for Type 304L in these tests lay below,

rather than between, the first two. This behavior may have been caused by the nitrate-containing solution. The original work was done in sulfuric acid. For this reason, this technique was not used.

### Instantaneous Corrosion Rates

Instantaneous corrosion rates for all ten test alloys in 10M $HNO_3$-0.01M HF were measured by the Stern-Geary Method[9] at approximately 20, 40, 60, 80, and 100°C. Corrosion rates as functions of temperature are summarized in Figure 1 for Hastelloy® C-276 and Inconel® 690, which define the upper and lower extremes, respectively. For the other alloys, only the 100°C data are shown. The best alloys (lowest corrosion rates) are Hastelloy® G, Haynes® 25, Inconel® 625, 671, 690, and Incoloy® 825. Ferralium®, Hastelloy® C-276, Haynes® 20, and Type 304L stainless steel exhibited the highest corrosion rates.

An instantaneous rate of 50 mils/year, which is about the average rate for the materials tested at 100°C, would normally indicate adequate corrosion resistance for most process equipment. All of the test alloys would be satisfactory below 90°C in 10M $HNO_3$ containing no more than 0.01M HF.

For 10M $HNO_3$ - 0.1M HF, instantaneous corrosion rates were measured only at 100°C. Figure 2 shows that although there are some secondary alloying effects, nickel-base alloys should contain at least 20% chromium for adequate corrosion resistance to solutions containing small amounts of $F^-$ and high concentrations of $HNO_3$. Comparison of Figures 1 and 2 indicates that, at 100°C, increasing the HF from 0.01M to 0.1M had a large effect on corrosion rates but little effect on the relative order of corrosion resistance for these alloys.

These data indicate that when the $F^-$ exceeds about 0.01M it must be complexed to reduce corrosion rates.

## Corrosion Tests of Coupons in $HNO_3$-HF Solutions

### Matrix Metal

Isothermal corrosion rates of the high nickel-chromium alloys were measured in 10M $HNO_3$ containing either 0.01M or 0.1M HF. The solutions were maintained at a constant 95°C. Coupons (1 by 2 by 1/8 in.) were exposed for 120 hours during which the solution was changed three times. The ratio of liquid volume to sample surface was 30 mL per $cm^2$. Weight losses ranged from 0.06 to 6.6 g per sample. Corrosion rates are summarized in Table 2. Results of these tests generally agree very well with results of the electrochemical tests.

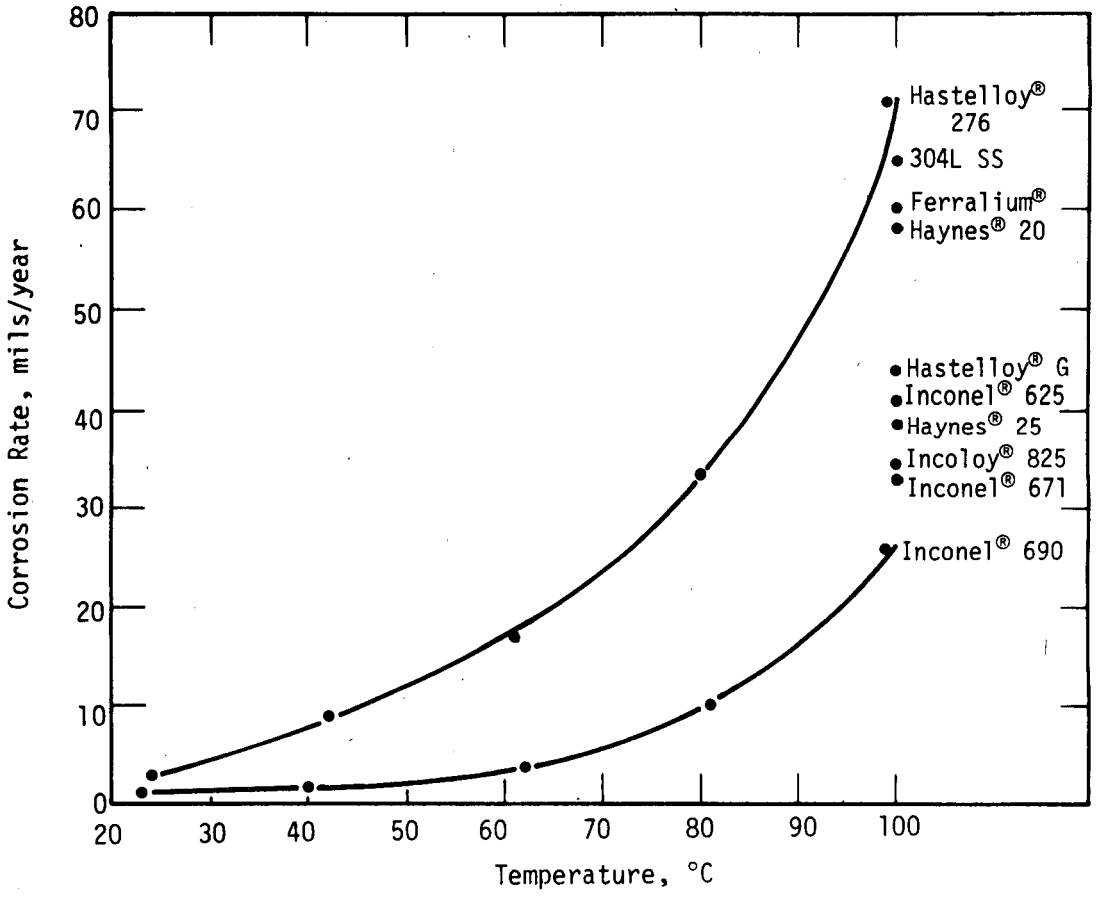


FIGURE 1. Instantaneous Corrosion Rates of High Ni-Cr Alloys in 10M $HNO_3$ - 0.01M HF

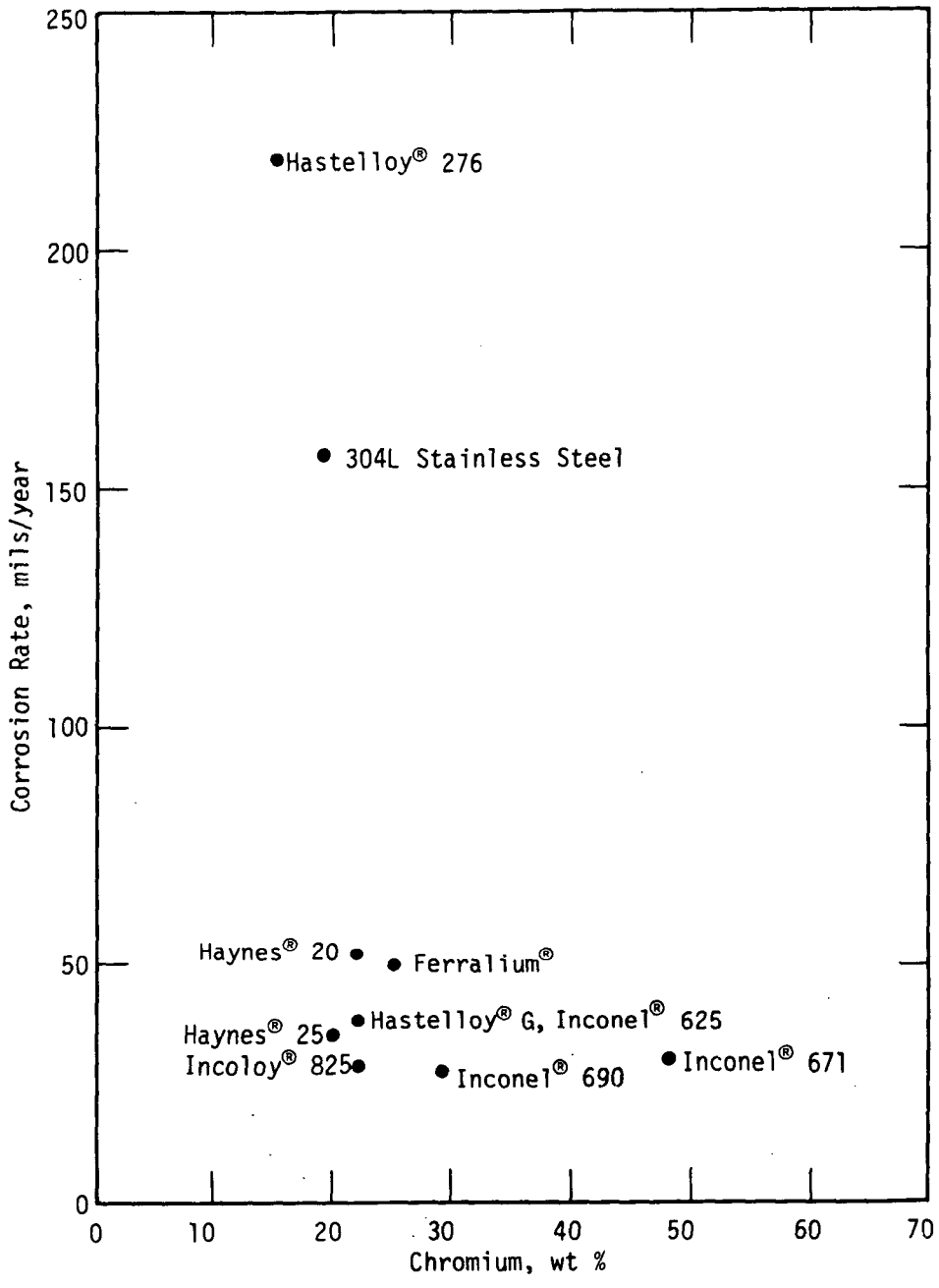


FIGURE 2. Effect of Chromium Content on Instantaneous Corrosion Rate of High Ni-Cr Alloys in 10M $HNO_3$ - 0.10M HF at 100°C

TABLE 2

Isothermal Corrosion Rates at 95°C*

| Alloy | Penetration Rate, mils/year Matrix Wrought Alloy 10M $HNO_3$-0.01M HF | 10M $HNO_3$-0.1M HF | Welded Alloy 10M $HNO_3$-0.1M HF | 12M $HNO_3$-0.05M HF |
|---|---|---|---|---|
| Inconel® 671 | 8 | 41 | 45 | 31 |
| Inconel® 690 | 9 | 63 | 68 | 53 |
| Haynes® 25 | 19 | 92 | 86 | 63 |
| Hastelloy® G | 18 | 138 | 220 | 140 |
| Inconel® 625 | 18 | 147 | 170 | 120 |
| Ferralium® | 19 | 157 | 140 | 96 |
| Incoloy® 825 | 28 | 206 | 230 | 140 |
| Haynes® 20 | 46 | 239 | 250 | 200 |
| Type 304L Stainless Steel | 21 | 248 | 190 | 100 |
| Hastelloy® C-276 | 134 | 841 | 760 | 530 |

*Coupons tested for 120 hours at 30 mL/cm$^2$. Solutions changed three times.

Instantaneous corrosion rates, measured electrochemically, generally ranked the alloys in the same order as indicated in Table 2. The three alloys with the lowest corrosion rates were Inconel® 671, Inconel® 690, and Incoloy® 825. The three alloys with the highest corrosion rates were Haynes® 20, Type 304L stainless steel, and Hastelloy® C-276. However, the initial instantaneous corrosion rates were higher than the average corrosion rates in 10M $HNO_3$-0.01M HF but lower than the average in 10M $HNO_3$-0.1M HF. These differences are attributed to changes in rates over the test period.

Alloys with average corrosion rates <50 mils/year are considered adequate for the test conditions (Table 2). Only one alloy, Inconel® 671, meets this criterion in $10M_3$-0.1M HF.

The surface appearance of two alloys representing extremes in corrosion resistance are compared in Figure 3. Hastelloy® C-276 had a very high penetration rate because attack was intergranular and a small amount grain dropping occurred. The surface of Hastelloy® C-276 is much rougher than that of Inconel® 690.

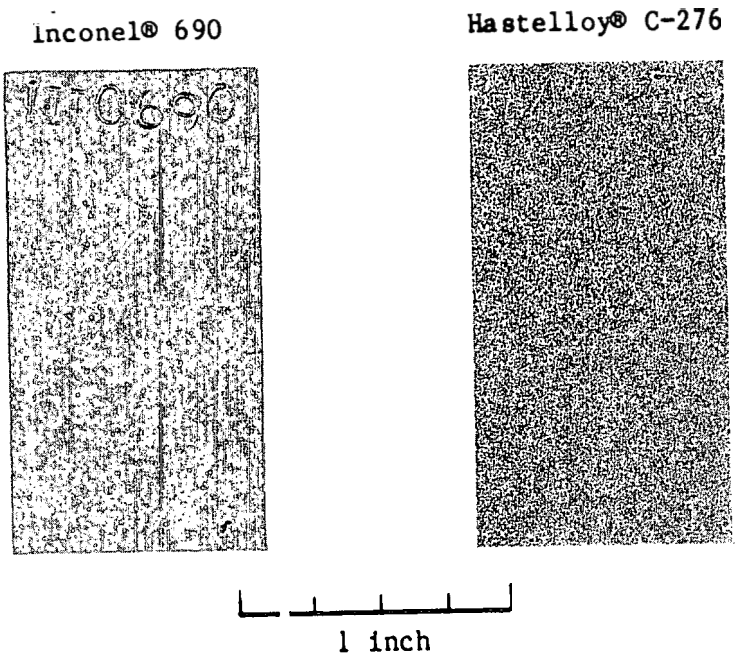


FIGURE 3. Typ cal Surface Attack of High Ni-Cr Alloys by 10M $HNO_3$-0.1M HF at 95°C

## Weld Zones

In aggressive solutions, nickel-chromium alloys sometimes exhibit intergranular corrosion in the heat-affected zone of welds. Welded samples typically have corrosion rates higher than wrought samples because weld metal or weld heat-affected zones are attacked more rapidly. To check for weld-zone effects, corrosion rates of butt-welded samples of all of the alloys were measured in uncomplexed solutions. The test procedures were similar to those for base metal. Samples were 1 by 3 by 1/8 inch with a 1-inch-long transverse weld corrosion was sometimes slightly higher in the heat-affected zone or in the weld metal (Table 2).

The data show that the corrosion rate for welded alloys is about 10% higher than that for wrought alloys under equivalent conditions. In tests at 95°C without complexing agents, only Inconel® 671 has an acceptable penetration rate (less than 50 mils/year). Above 95°C, even Inconel® 671 would probably be inadequate.

Typical weld zone attack is illustrated for two of the samples in Figure 4. Exposure was for 6 days at 95°C to 10M $HNO_3$-0.1M HF. Under these same conditions, attack on wrought metal was uniform. Inconel® 690 showed slight intergranular attack along the heat-affected zone and some weld metal attack. The worst preferential attack was for Hastelloy® G, where weld metal was pitted to a depth of about 7 mils, and intergranular attack in the heat-affected zone was 3 to 4 mils deep.

## Effect of Complexing Agents for Fluoride Ion

One method of predicting the relative effectiveness of ions in reducing corrosion is to compare stability constants of the ion-fluoride complexes. A larger constant indicates that a given ion is more effective in reducing corrosion. Data for several potential complexing ions are shown in Table 3.

Stability constants in Table 3 range from about $10^3$ for $H^+$ to $10^{10}$ for $Zr^{4+}$. However, this does not mean that corrosion will be reduced proportionately, for example, by a factor of $10^7$ in a $Zr^{4+}$-complexed solution compared to an $H^+$-complexed solution at the same concentration. The stability constants are calculated specifically for the binary solutions extrapolated to zero ionic strength. In actual corroding systems, many other ions are present that alter the chemical equilibria significantly. However, the constants are a measure of the strength of the respective complexes and are expected to indicate the order of effectiveness of the complexing ions.

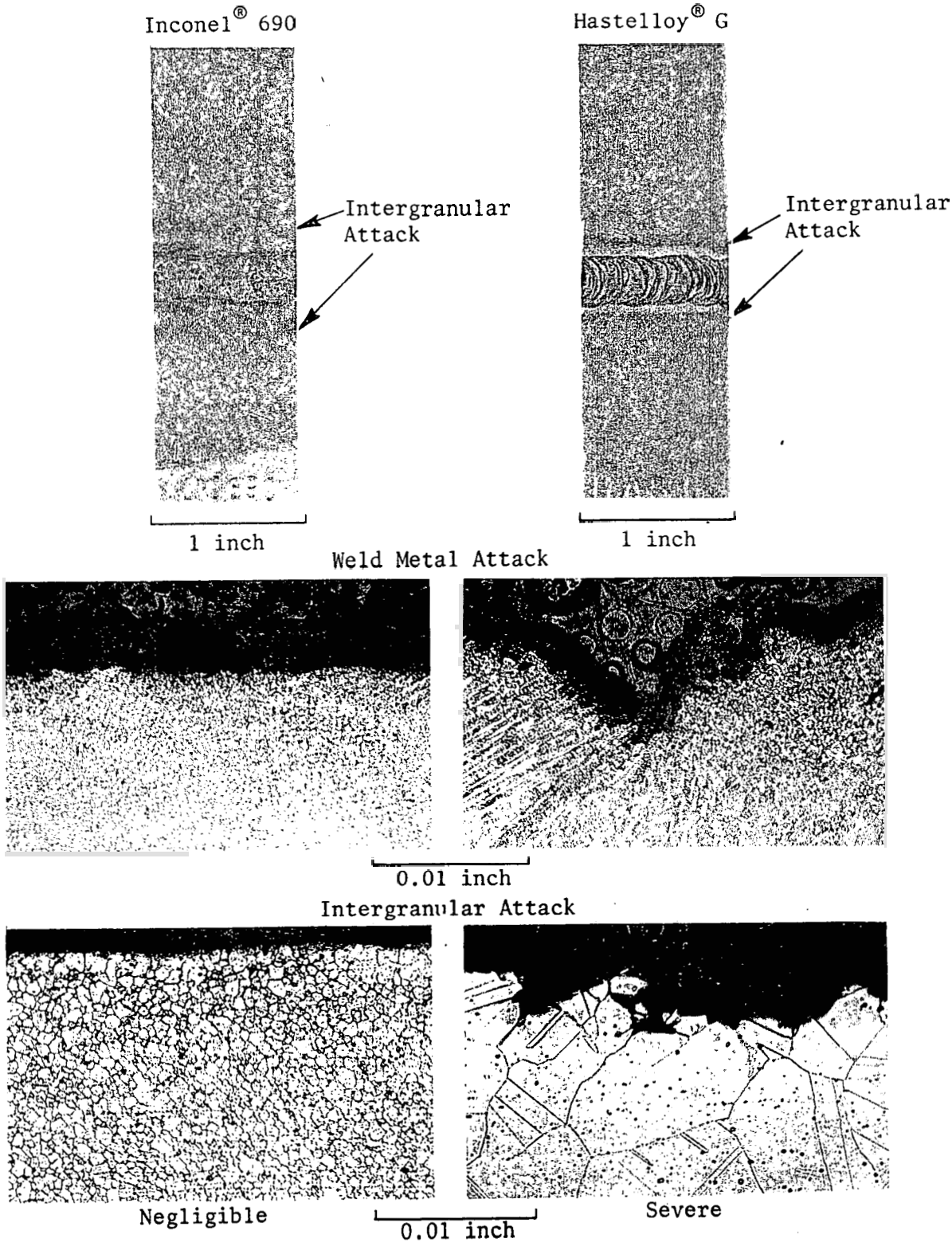


FIGURE 4. Extremes of Weld Area Attack

TABLE 3

Stability Constants* of Fluoride Complexes[11]

| *Complexing Ion* | *Log of Stability Constant*** |
|---|---|
| $H^{+}$ | 3.1 |
| $Al^{3+}$ | 7.0 |
| $Th^{4+}$ | 8.6 |
| $Zr^{4+}$ | 9.8 |

*Stability Constant = $\frac{[\text{complex}]}{[F^-]\ [\text{complexing ion}]}$

**At zero ionic strength and 25°C.

To evaluate the effects of complexing agents, the corrosion rates of duplicate samples of the same test alloys were measured first in solutions with no complexing agent, then in solutions with increasing concentrations of complexing agent. Except for Hastelloy® C-276, the corrosion rates were rapidly reduced to acceptable rates (<50 mils/year).

Figures 5, 6, and 7 show the effects of the complexing ions in 10M $HNO_3$-0.1M HF solutions at 95°C. The reduction in corrosion rate is nonlinear with concentration and slightly different for each alloy. For example, to achieve a corrosion rate of 20 mils/year for Type 304L, the effectiveness is in the ratio of 1/1/2 for $Zr^{4+}/Th^{4+}/Al^{3+}$; for Inconel® 671, it is 1/1/4. Generally, the ratio of complexing ions required to get the same corrosion rate is about 1/1/2.5 for $Zr^{4+}/Th^{4+}/Al^{3+}$.

Complexing agents would be required for dissolution of $ThO_2$, $HNO_3$ recovery, and waste storage. $Th^{4+}$could be used in the dissolver as a complexing agent, but it would be removed from the solution during extraction and would not follow the $F^-$ into $HNO_3$ recovery and waste storage. Therefore, $Zr^{4+}$ or $Al^{3+}$ would have to be added even though waste volume would be increased.

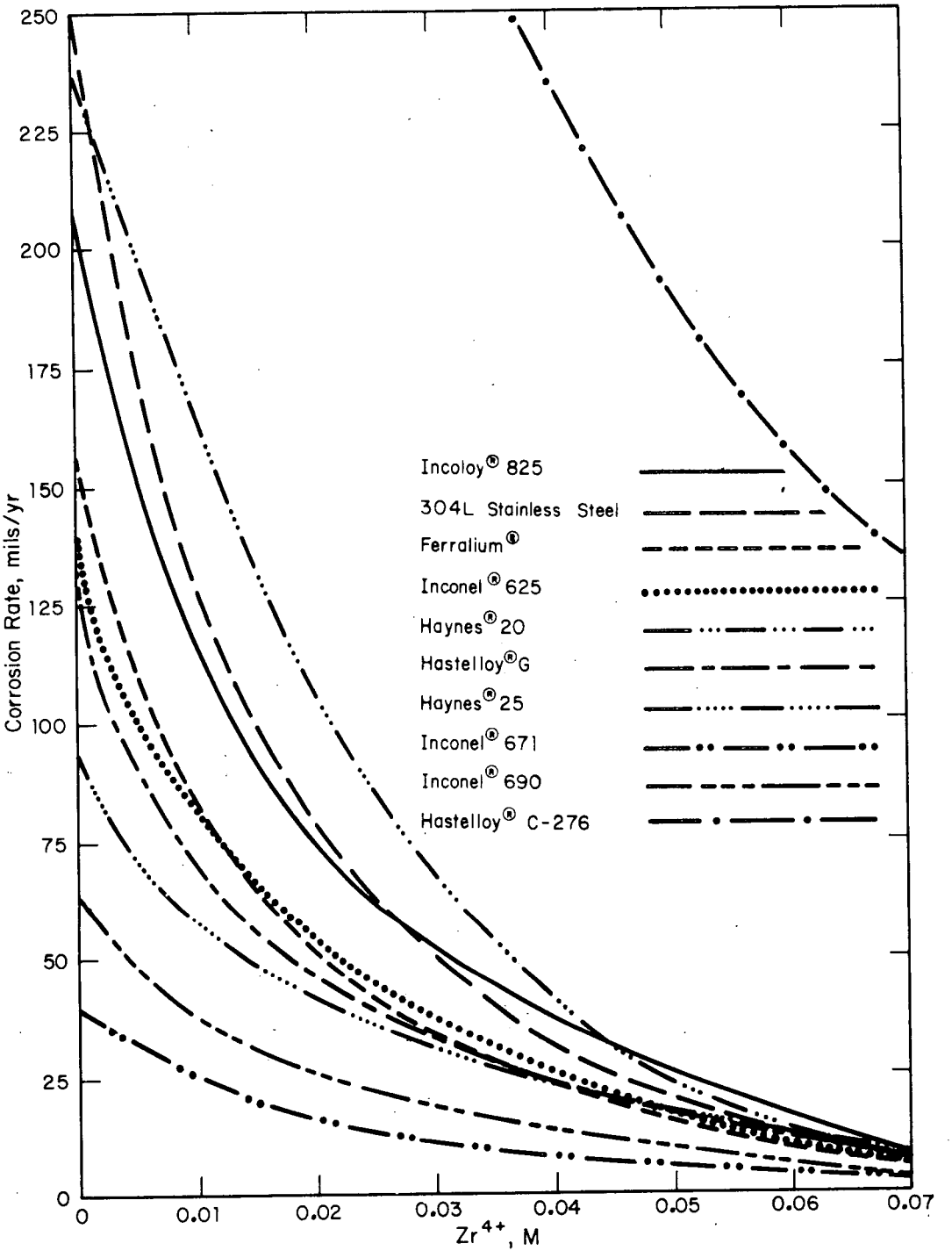


FIGURE 5. Corrosion of High Ni-Cr Alloys in 10M $HNO_3$-0.1M HF-$Zr^{4+}$ at 95°C

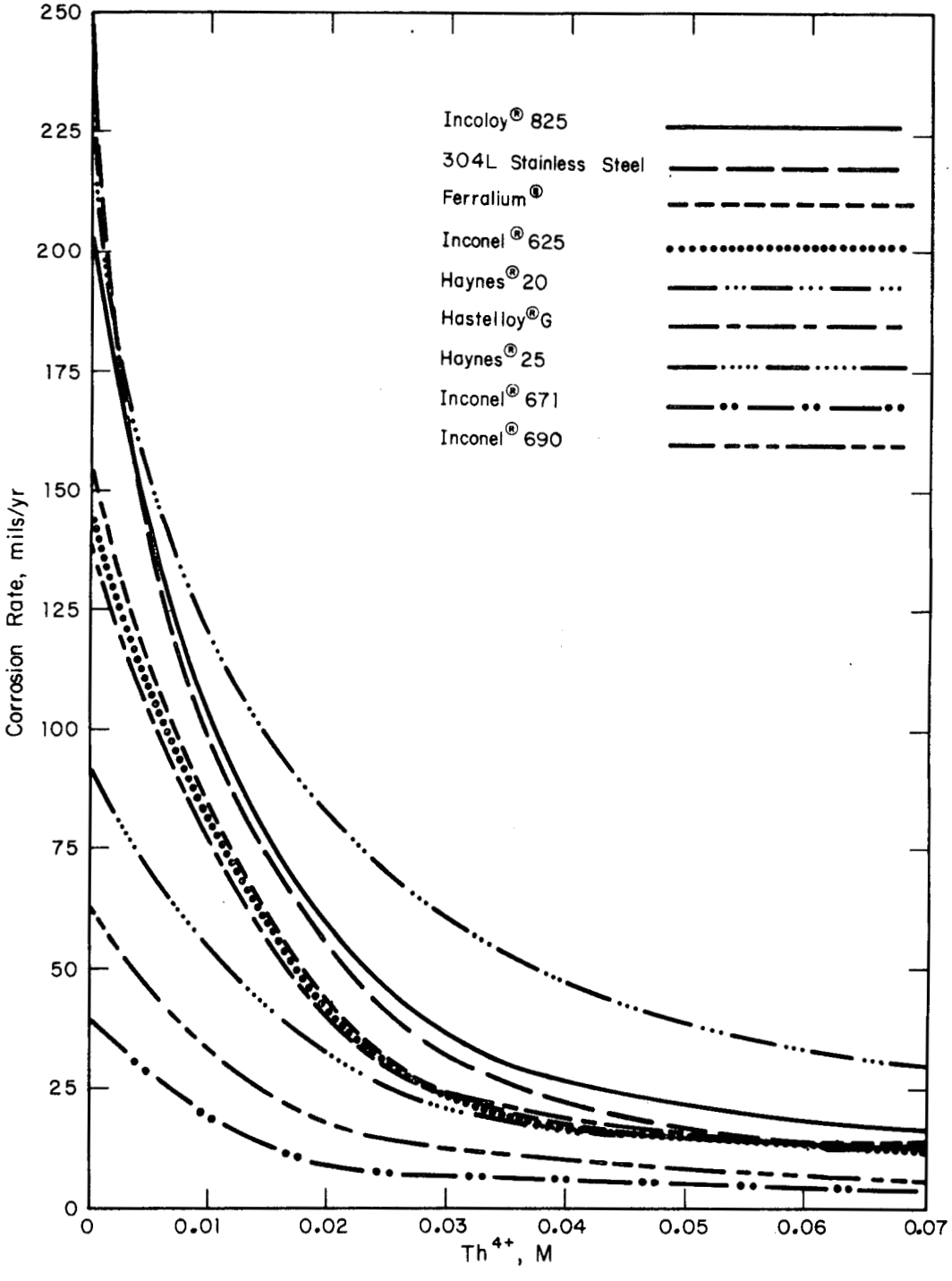


FIGURE 6. Corrosion of High Ni-Cr Alloys in 10M $HNO_3$-0.1M HF $Th^{4+}$ at 95°C

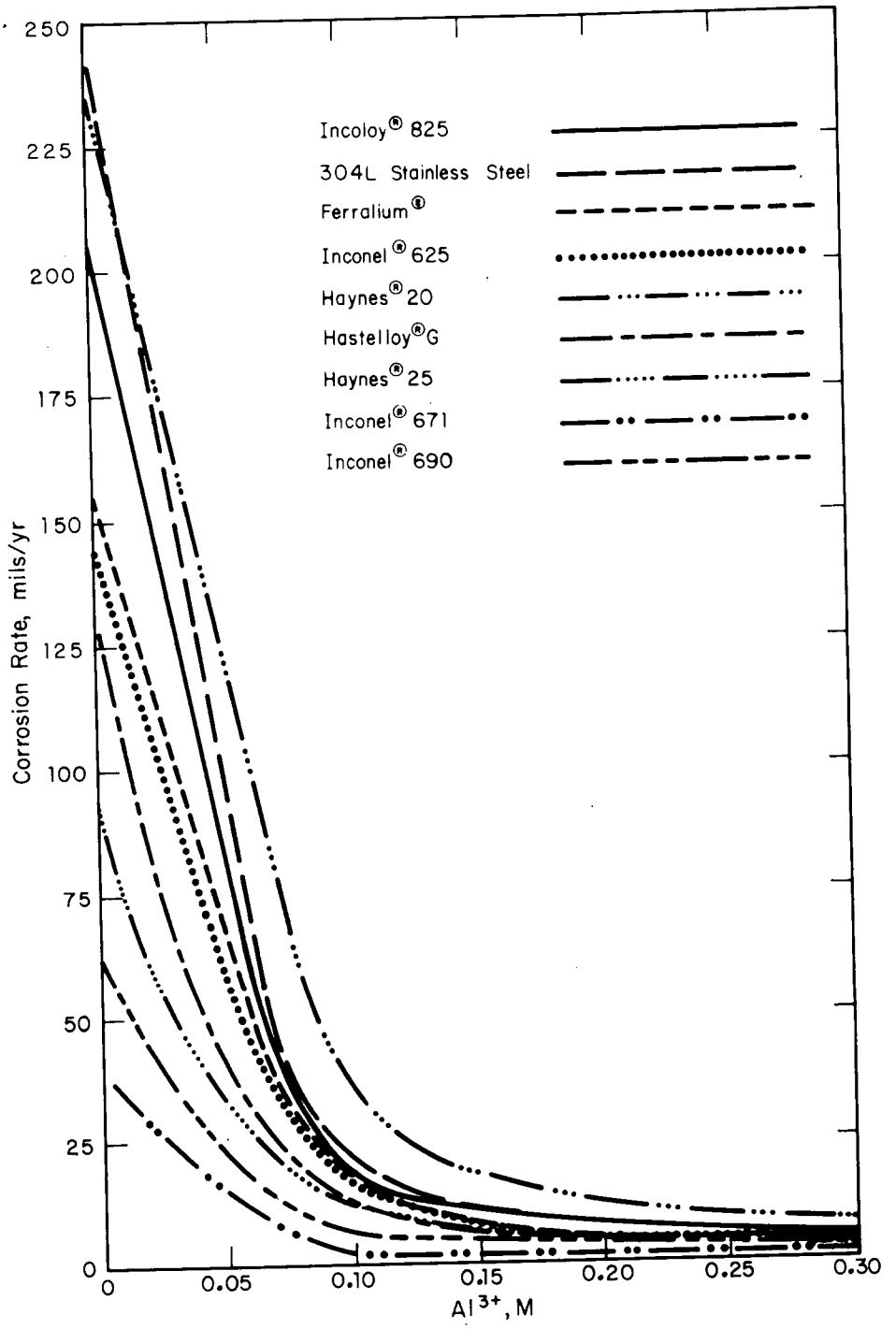


FIGURE 7. Corrosion of High Ni-Cr Alloys in 10M $HNO_3$-0.1M HF $Al^{3+}$ at 95°C

High concentrations of complexing agents may retard thorium oxide dissolution unacceptably. Studies of thorium oxide dissolution showed that about 13M $HNO_3$ was optimum and that $F^-$ accelerated dissolution although $ThF_4$ precipitated when HF was above 0.1M.[12] Adding a complexing agent to inhibit corrosion rates may also tie up much of the free $F^-$ that was added to accelerate dissolution. As a compromise, proposed plant dissolver conditions were set at 12M $HNO_3$ and 0.025M HF, with 0.1M $Al^{3+}$ to inhibit corrosion.

The particle size of $ThO_2$ had a very large effect on the dissolution rate, smaller sizes being dissolved more rapidly. The method of producing $ThO_2$ also greatly affected dissolution rates. If large amounts of complexing ion are required to reduce corrosion, the small-particle-size $ThO_2$ made by the sol-gel process will give the highest plant throughput.

Corrosion rates of the test alloys were also measured at 95°C in the proposed dissolver solution, 12M $HNO_3$-0.05M $HF^-$ 0.025M $Zr^{+4}$. These data, summarized in Table 4, confirm that except for Hastelloy® C-276, all the alloys have acceptably low penetration rates.

TABLE 4

Corrosion Rates at 95°C in Proposed $ThO_2/UO_2$ Dissolver Solution*

| *Alloy* | *Penetration Rate, mils/year* |
|---|---|
| Inconel® 671 | 2 |
| Inconel® 690 | 4 |
| Haynes® 25 | 10 |
| Hastelloy® G | 10 |
| Ferralium® | 11 |
| Inconel® 625 | 12 |
| Type 304L | 13 |
| Incoloy® 825 | 15 |
| Haynes® 20 | 19 |
| Hastelloy® C-276 | 190 |

*12M $HNO_3$-0.05M HF-0.025M $Zr^{4+}$

The data show that many of the Ni-Cr, Ni-Cr-Fe, or Co-Cr alloys would be suitable for the $ThO_2/UO_2$ dissolver if complexing agents were used. Of the ten test alloys, Hastelloy® C-276 (Table 4) is not satisfactory because of its high corrosion rate and Hastelloy® G because of preferential attack at welds, Figure 4. In addition to the eight alloys that were successfully tested, Inconel® 601 and 617, Hastelloy® X, Haynes® 188, and Types 309 and 310 stainless steels would also be adequate, based on their composition.

Based on corrosion resistance alone, Inconel® 671 would probably be selected as the material for the dissolver and off-gas system; its cost is about $8/lb. If selection is based on corrosion resistance plus cost, probably Inconel® 690 at $6/lb might also be adequate if enough complexing agent is always present and no process upsets occur. If process upsets result in insufficient complexing agent, enough $Fe^{3+}$ and $Cr_2O_7^{2-}$ could be formed to accelerate preferential attack of equipment downstream.

## Tests at Elevated Temperature

Tests in an autoclave lined with Teflon® (Du Pont) have shown that addition of either $Zr^{4+}$ or $Th^{4+}$ to the reference dissolver solution lowers corrosion rates sufficiently to permit several high Ni-Cr alloys to be used for steam coils in the dissolver. Steam coils are expected to be the most rapidly attacked portions of dissolvers because they have the highest surface temperature and because of the heat transfer across their walls.

Figures 8 and 9 summarize attack rates on all the test alloys, by the proposed dissolver solution (12M $HNO_3$-0.05M HF-0.025M $Zr^{4+}$) at 130°C, as a function of complexing ion concentrations. Based on stability constants, the complexing ability of $Zr^{4+}$ is expected to be about 10 times that of $Th^{4+}$. In fact, $Zr^{4+}$ proved to be about eight times as effective as $Th^{4+}$. Concentrations of either 0.075M $Zr^{4+}$ or 0.5M $Th^{4+}$ were required to protect most of the alloys at 130°C. At 0.075M $Zr^{4+}$, corrosion is reduced to a minimum, and the amount added from 0.075M to 0.125M $Zr^{4+}$ produced no further reduction.

Inconel® 671 is the best alloy tested when no fluoride complexing agents are present; Inconel® 690 is the best with complexing agents. Both are superior to the other alloys tested at 130°C when flouride complexing agents are at low concentrations. Therefore, during a process upset, 671 and 690 would be attacked the least. Ferralium®, Inconel® 825, Haynes® 20, and 304L are useful at 130°C if 0.075M $Zr^{4+}$ or 0.5M $Th^{4+}$ are present in the dissolver solution. The corrosion rates of Inconel® 625 and Hastelloy® G are too high; these alloys are not recommended for steam coils. Haynes® 25 does not meet the minimum requirements (less than 50 mils/year) and would add an excess of corrosion products to the dissolver solution.

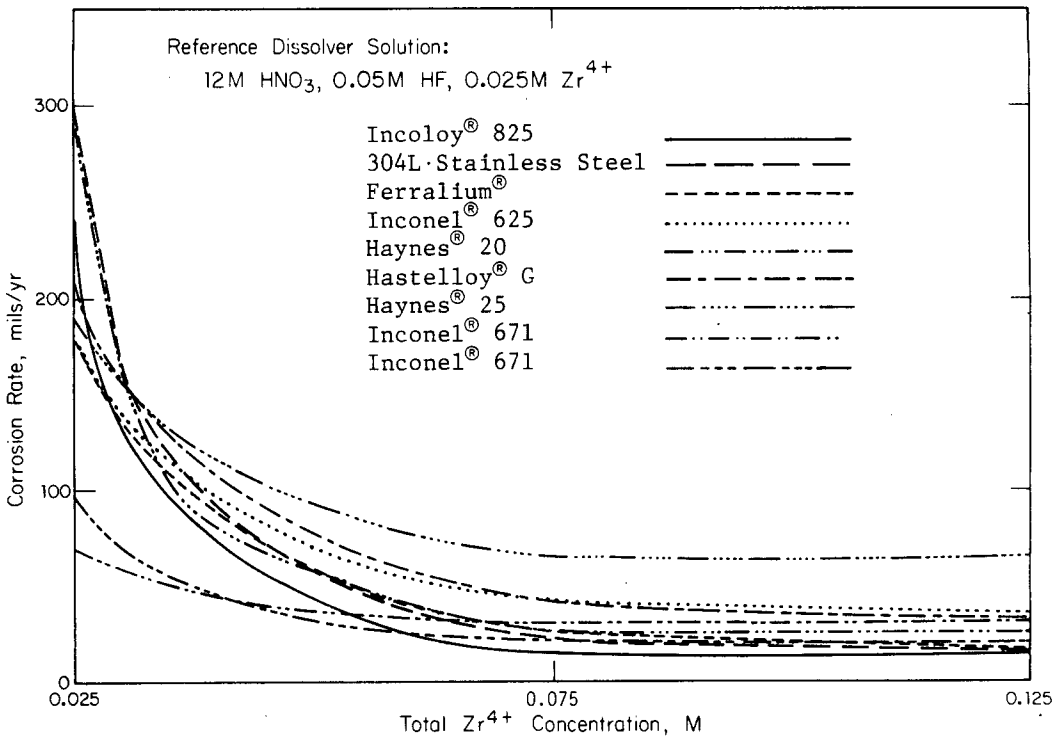


FIGURE 8. Effect of $Zr^{4+}$ Additions on Corrosion of Candidate Alloys in Thorium Oxide Dissolver Solutions at 130°C

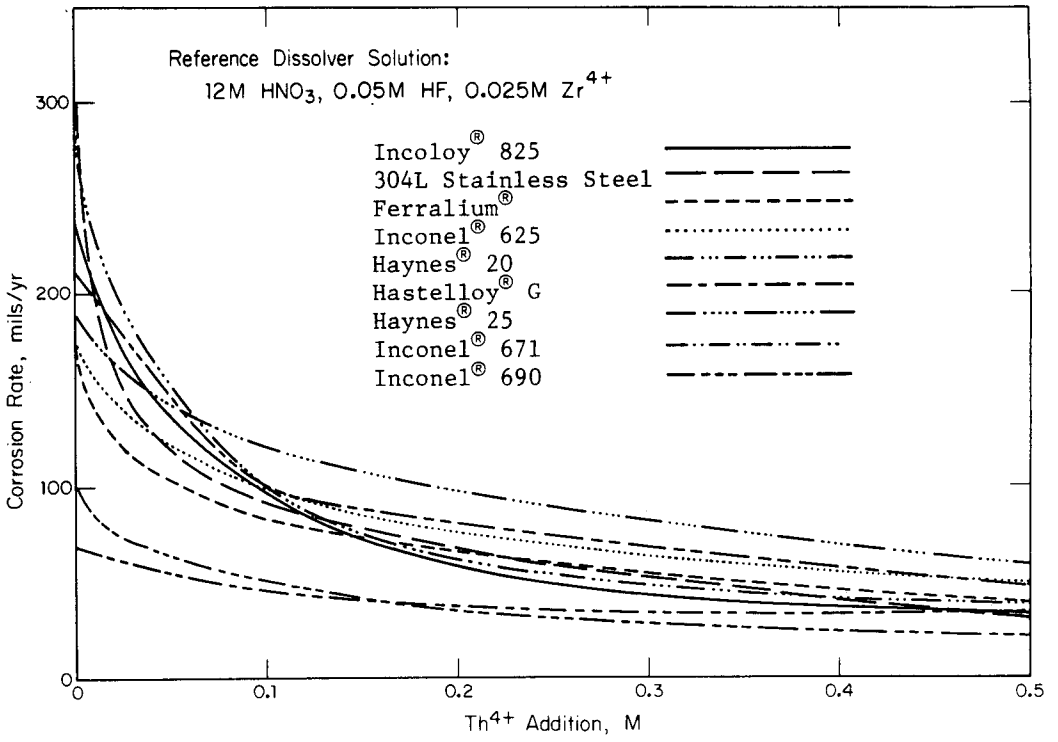


FIGURE 9. Effect of $Th^{4+}$ Additions on Corrosion of Candidate Alloys in Thorium Oxide Dissolver Solution at 130°C

Corrosion Rates Under Plant Conditions

Three alloys tested for corrosion rates in the presence of complexing agents were also tested electrochemically in solutions duplicating previous plant conditions for dissolution of $ThO_2$. Figure 10 shows corrosion rates in 12M $HNO_3$-0.025M HF-0.1M $Al(NO_3)_3$-0.5M $Th(NO_3)_4$ from room temperature to just below the solution boiling point. In 12M acid near the boiling point, Type 304L stainless steel corroded slightly faster than either Ferralium® or Inconel® 690 when the $Al^{3+}$ concentration was four times the $F^-$ concentration.

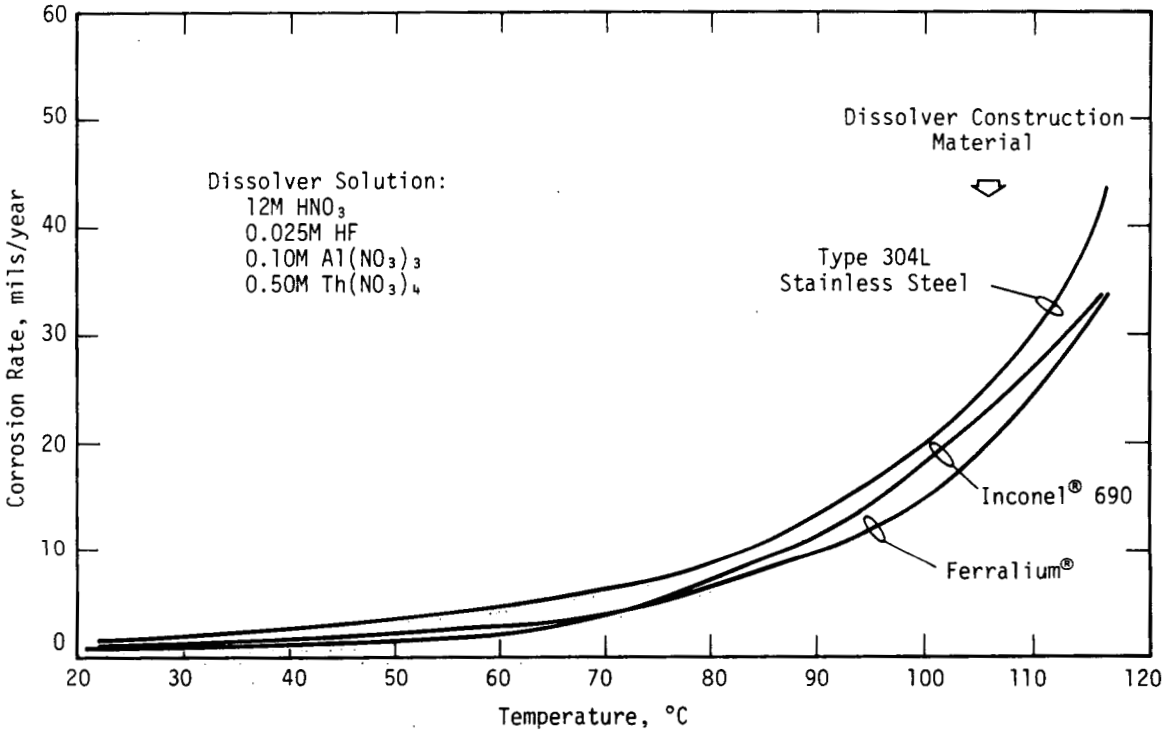


FIGURE 10. Instantaneous Corrosion Rates Under Plant Conditions

## EVALUATION OF TYPE 304L STAINLESS STEEL FOR USE WITH URANIUM FUELS

### Polarization Evaluation

An electrochemical study of the behavior of Type 304L stainless steel in 10M $HNO_3$-0.01M HF at room temperature indicates that 304L is probably acceptable as the principal material of construction for a reprocessing facility for uranium reactor fuels. The open-circuit corrosion rate in an air-saturated solution was calculated to be 4 mils/year, which is consistent with coupon (weight loss) tests but is about twice that predicted by linear polarization. Anodic polarization causes the 304L to behave more like an active metal, which would probably make it less resistant to corrosion. Film formation during potentiostatic polarization is characterized by a current-time transient typical of metals that passivate by ionic transport through the oxide with a very slow buildup in film thickness. Cyclic potentiodynamic anodic polarization indicates that breakdown and protection potentials cannot be distinguished clearly.

### Steady-State Potentiostatic Polarization

Figure 11 shows two steady-state potentiostatic polarization curves. Each point on the curves in Figure 11 represents an individual specimen that was polarized at the indicated potential until steady state was achieved. For example, Figure 12 shows the approach to steady state for a sample at 850 mV. These curves in Figure 11 are, therefore, suitable for predicting corrosion rate under conditions of long-term polarization.

The "nonwelded" curve was obtained with 2-inch-long, 0.16-inch-diameter cylinders of Type 304L stainless steel. The "welded" curve was obtained with specimens of the same dimensions but with about 0.4 inch of Type 308 stainless steel weld metal in the center. This weld metal is not visible prior to anodic polarization but becomes evident after polarization into the transpassive range of 304L which can cause etching or pitting.

As shown in Figure 11, the corrosion potential (open circuit potential) of freshly polished Type 304L stainless steel in hydrogen-saturated 10M $HNO_3$-0.01M HF is at steady state near 755 mV (vs. a saturated calomel electrode). In air-saturated 10M $HNO_3$-0.01M HF, the steady-state value is near 800 mV. This

difference is attributed to the reaction $O_2 + 4H^+ + 4e^- \rightarrow 2H_2O$, which contributed to the reduction process in air. In the absence of oxygen, however, reduction is controlled entirely by the reaction $2H^+ + 2e^- \rightarrow H_2$.

During potentiostatic polarization in these tests, film formation was characterized by a current vs. time transient (Figure 12) typical of metals that passivate by ionic transport through the oxide.[13] The solution current reached steady state, which indicates that the film was thickening very slowly.

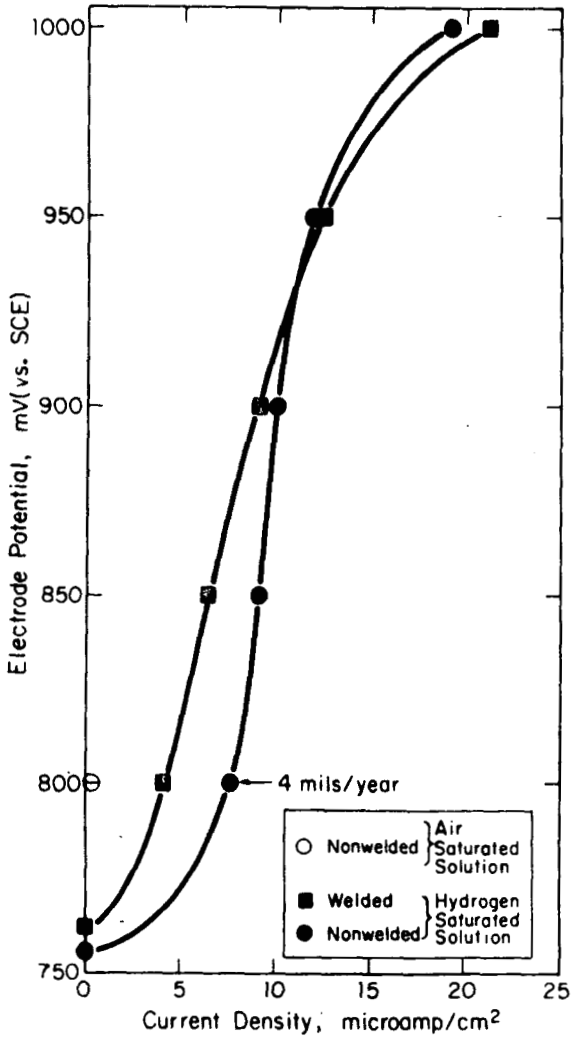


FIGURE 11. Steady-State Potentiostate Polarization Curves for Welded and Nonwelded Specimens of Type 304L Stainless Steel in 10M $HNO_3$-0.01M HF

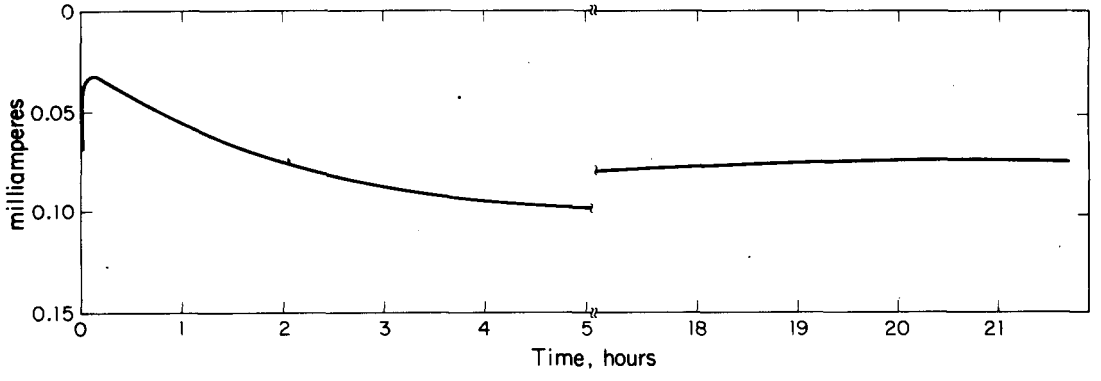


FIGURE 12. Current vs. Time Transient of Type 304L Stainless Steel at 850 mV

The steady-state curve for pure 304L can also be used to estimate the open-circuit corrosion rate in an air-saturated solution. This steady-state curve is representative of 304L in oxygen-free 10M $HNO_3$-0.01M HF. In oxygen-free acid solution, the cathodic current density ($i_c$) can be totally attributed to the reduction of hydrogen ions. At the corrosion potential, $E_c/H_2$ (755 mV), the net external current density (i) is zero. Thus, $i = i_A - i_c = 0$, where $i_A$ is the current density for anodic dissolution. At potentials more positive than $E_c/H_2$, the contribution of $i_c$ to i decreases exponentially so that at 800 mV, it can be assumed to equal $i_A$. If $i_A$ is a function only of the electrode potential and not the gas with which the solution is saturated, then at 800 mV, $i_A$ (in air) = $i_A$ (in hydrogen) = $7.7 \times 10^{-6}$ amp/cm$^2$.

Because 800 mV is the open-circuit potential in air, the open-circuit anodic dissolution current in air is $7.7 \times 10^{-6}$ amp/cm$^2$. The corrosion rate (R) in cm/sec can then be calculated with

$$R = \frac{i_A K}{\rho F}$$

where $K = \sum_{\alpha} m_\alpha \frac{M_\alpha}{n_\alpha}$

and $i_A$ = anodic current density = $7.7 \times 10^{-6}$ amp/cm$^2$

$\rho$ = alloy density = 8 g/cm$^3$ for Type 304L

F = Faraday constant = 96,500 coulombs/equivalent

$m_\alpha$ = mass fraction of constituent $\alpha$

$M_\alpha$ = mole weight of $\alpha$

$n_\alpha$ = equivalents for $\alpha$ per mole

K = g/equivalent = 32.3 for Type 304L

Results indicate that $R = 3.21 \times 10^{-10}$ cm/sec or 4 mils/year. This is more than twice the open-circuit corrosion rate predicted by linear polarization.[2] However, coupon tests at elevated temperatures have consistently given corrosion rates 2 to 4 times greater than those predicted by linear polarization at the same temperatures. Therefore, linear polarization does not appear to be the most accurate technique for predicting the open-circuit corrosion behavior of 304L in solutions of nitric and hydrofluoric acids, probably because linear polarization is a rapid scan technique which does not permit the electrode-solution interface to approach steady state.

## Cyclic Potentiodynamic Anodic Polarization

Several methods are commonly used to measure the resistance of stainless alloys to pitting. One of the more popular methods is cyclic potentiodynamic anodic polarization. In this method, the alloy is immersed and polarized to increasingly higher potentials with a potentiostat. A potential is eventually reached at which the passive film on the metal surface breaks down locally and pitting begins. This breakdown potential is marked by a sudden increase in the polarizing current. Polarization is continued into the transpassive range. At some preselected potential (1500 mV in this case) or current density, the direction of scan is reversed. If the alloy is susceptible to pitting, the potential is lower at a given current (negative) hysteresis) during the descending scan, and the point where the descending curve intersects the ascending curve locates the protection potential. This potential is usually more active than the breakdown potential and marks the potential below which growing pits repassivate and no new pits initiate.

The cyclic polarization curve at 2/3 mV per second shown in Figure 13 indicates a protection potential near 1000 mV (vs. a saturated calomel electrode); the breakdown potential is also near 1000 mV (Figure 13). Thus, the distinction between breakdown potential and protection potential has no practical significance for this particular electrochemical system. After cyclic polarization, the surface of the specimen was examined on the scanning electron microscope; a typical region is shown in Figure 14. The surface has an etched appearance with many isolated pits not associated with grain boundaries.

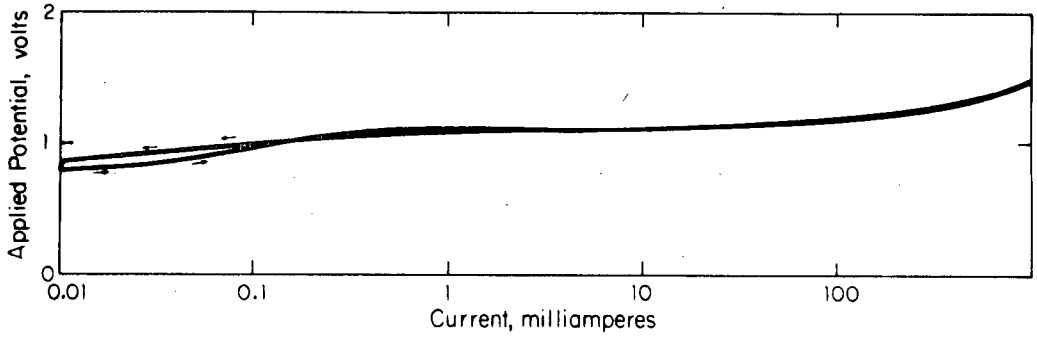


FIGURE 13. Cyclic Polarization Curve for Type 304L Stainless Steel in Hydrogen-Saturated 10M $HNO_3$-0.01M HF

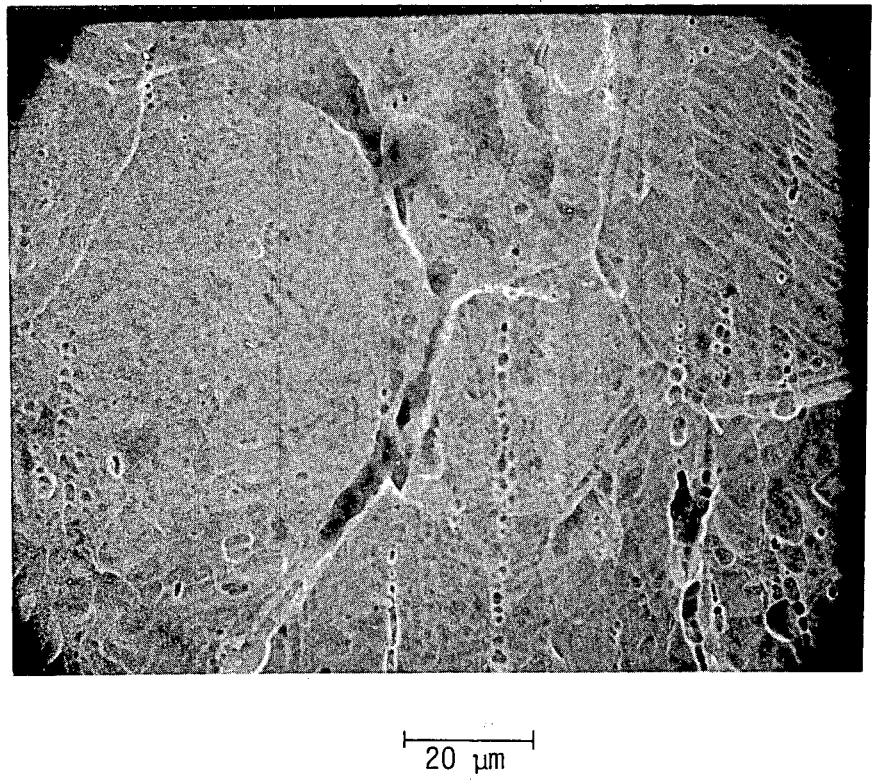


FIGURE 14. Surface of Type 304L Stainless Steel After Cyclic Polarization

## Passivity of Type 304L Stainless Steel in $HNO_3$-HF

Electrochemical tests determined the concentrations of $HNO_3$-HF in which 304L would be in the passive state, the ideal metallic state for process equipment. Metals are usually in the active or passive states depending on their electrode potential.

A potentiodynamic polarization curve is shown in Figure 15 for 304L in 0.2M $F^-$. The shape of the curve indicates that the metal is in the active range and will corrode at a comparatively rapid rate. If the metal is raised to the passive state, such as by increasing its electrode potential, the corrosion rate would decrease (as shown by the lower current density in this span).

Additions of $HNO_3$ to HF increased the open circuit potential to a positive value and changed the shape of the polarization curve indicating passivity and, therefore, reduced corrosion, as shown in Figure 16. Note that the open circuit potential and majority of the curve is in the passive range of Figure 15. The boundary between the active and passive states as a function of $HNO_3$-HF concentration is shown in Figure 17. This boundary shows the minimum $HNO_3$ concentration needed in an HF solution to produce the passive state for 304L. At this boundary, a sharp change (about 0.5 V) in electric potential was observed.

## Electrochemical Tensile Test[14]

Electrochemical tensile test results confirmed that 304L would be damaged if it were not in the passive state. In this test, the alloy sample is made the anode of an electrochemical cell with the experimental solution as an electrolyte. The cathode is a platinum counterelectrode, and the potential of the specimen is measured against a reference electrode. When the anode is strained in the tensile machine at about $10^{-6}$/sec, its potential is maintained constant with a potentiostat.

Test results in Table 5 show that the attack is most severe in the active-to-primary passive potential range with little attack in the other ranges (Figure 15). This behavior infers that anodic protection might be used in HF solutions to decrease corrosion rates just as it is in carbon steel tanks that contain low concentrations of sulfuric acid. It also confirms the observation that a strong oxidizing agent such as $HNO_3$ added to the solution forces the metal into the passive range and reduces corrosion.

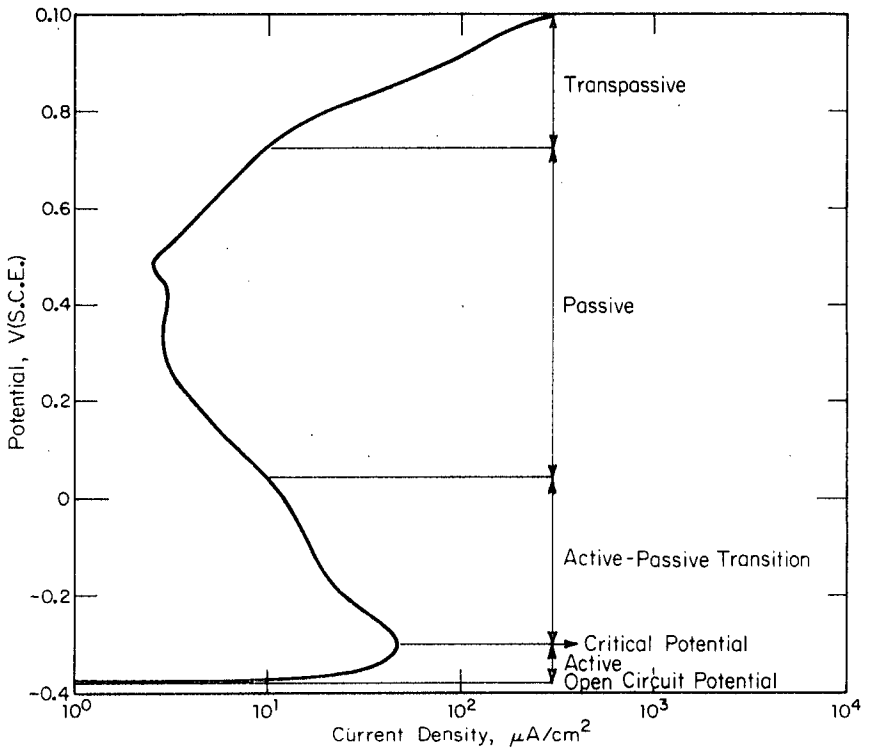


FIGURE 15. Anodic Potentiodynamic Polarization of Type 304L Stainless Steel in 0.2M HF

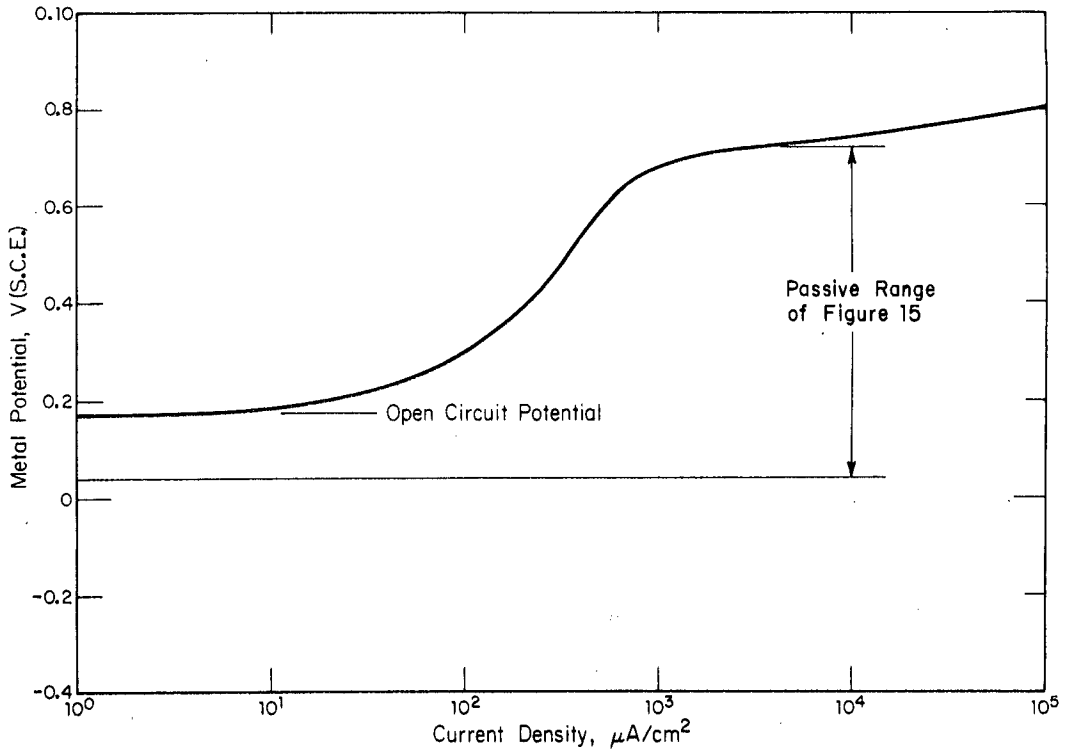


FIGURE 16. Anodic Potentiodynamic Polarization of Type 304L Stainless Steel in 8M $HNO_3$-0.2M HF

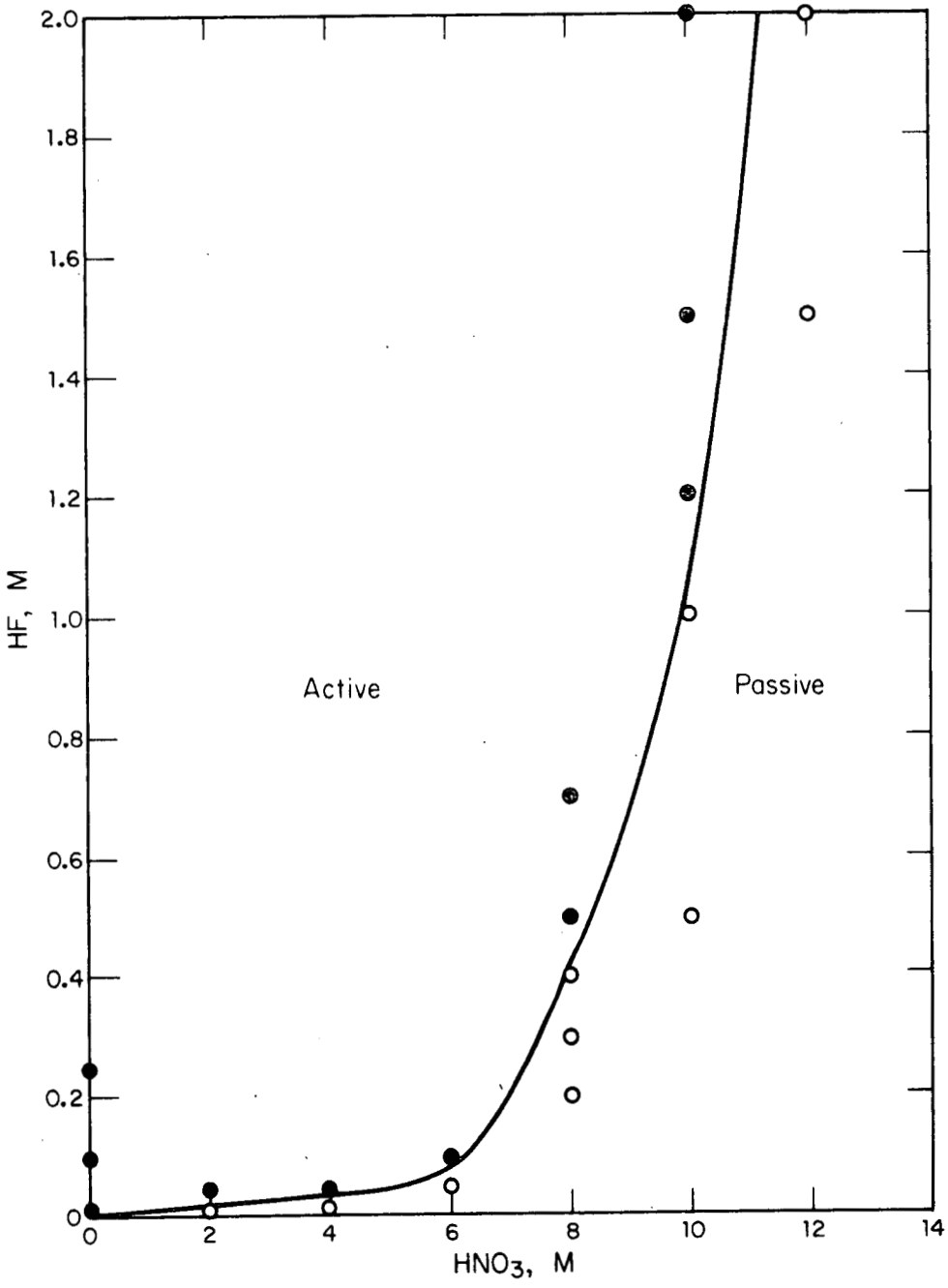


FIGURE 17. Summary of Potentiodynamic Polarization Data Indicating Active-Passive Behavior of 304L Stainless Steel in $HNO_3$-HF at 25°C

TABLE 5

Electrochemical Tensile Test

| *Polarization Potential,* V* | *Curve Section Potential* | *Elongation, %* | *Cracks* |
|---|---|---|---|
| Air (none) | - | 59 | No |
| -0.38 | Active | 57 | Yes |
| -0.35 | Active | 46 | Yes |
| -0.30 | Critical Potential | 57 | Yes |
| 0.0 | Active-Passive Trans. | 58 | No |
| +0.4 | Passive | 61 | No |
| +0.9 | Transpassive | 58 | No |

*Potential versus a saturated calomel electrode.

General Corrosion and Stress Corrosion Cracking Tests

The mixed $HNO_3$-HF solution is expected to be the most corrosive solution encountered in fuel reprocessing. Attack by $F^-$ must be limited because, in hot $HNO_3$, corrosion products form $Fe^{3+}$ and $Cr_2O_7^{2-}$, which then autocatalytically attack stainless steel. This could damage evaporators, waste tanks, and dissolvers. $Cl^-$ impurities in reagents might also cause corrosion but may be reduced by use of complexing agents. Stress-corrosion cracking of Type 304L stainless steel in $HNO_3$-HCl is not expected to be significant at the tested concentrations.

Possible Complexing Agents

Published stability constants showed that $Hg^{2+}$ could be used to complex $Cl^-$, but no such agent was found for $Cr_2O_7^{2-}$. Other ions that would be effective complexing agents for $Cl^-$ are rare and, therefore, expensive (Table 6). Fluoride ion complexing agents are summarized in Table 3.

TABLE 6

Stability Constants* of Chloride Complexes

| *Halide* | *Complexing Ion* | *Temp., °C* | *Log of Stability Constant* |
|---|---|---|---|
| $Cl^-$ | $Pd^{2+}$ | 38 | 5.9 |
| | $Tl^{3+}$ | 21 | 6.2 |
| | $Hg^{2+}$ | 25 | ∿7 |

$$*\text{Stability constant} = \frac{[\text{complex}]}{[\text{halide}][\text{complexing ion}]}$$

Corrosion Tests with Welded Specimens

The effectiveness of several complexing ions in diminishing stainless steel corrosion was determined at two temperatures and at two concentrations of $HNO_3$ (Table 7). These measurements were needed because stability constants are measured under ideal conditions. Test specimens consisted of two beveled pieces of Type 304L stainless steel welded together by Type 308 stainless steel (Figure 18).

Attack by $HNO_3$-HF. Test results showed that, of the solutions studied, uncomplexed HF alone in the nitric acid caused maximum attack. Pit depths in the 100-day tests commonly ranged from 100 to 600 μm (0.004 to 0.024 inch), and were occasionally deeper. In addition, a portion of the metal surface was lost by grain dropping. Corrosion attack was most severe with the 7M $HNO_3$ + 0.05M HF solution (Figure 19) and moderately severe with 3M $HNO_3$ + 0.05M HF (Figure 20). The attack initiated and was most pronounced on sample surfaces perpendicular to the rolling direction (end-grain attack) (Figure 19). In addition, the heat-affected zone of the 304L exhibited more extensive pitting than regions not affected by weld heating (Figure 20). The 308 filler metal in the weld exhibited negligible corrosion. The addition of 0.20M $Al(NO_3)_3$ to the $HNO_3$ + HF solution reduced, but did not eliminate, the pitting (Figure 21).

Weight loss measurements confirm that 0.05M HF in the synthetic reprocessing solutions caused severe corrosive attack on 304L. Table 8 shows weight loss in test solution relative to weight loss in 3M $HNO_3$. This attack was reduced to low values (1 to 10 mils/year) by complexing the $F^-$ with an equivalent concentration of $Zr^{4+}$.

TABLE 7

Corrosion of Type 304L Stainless Steel Specimens Welded Together with Type 308 Stainless Steel

| *Solution Composition, M** | | | | | | | | | *Specimen Weight Loss, After 100 Days, grams,** at* | |
|---|---|---|---|---|---|---|---|---|---|---|
| $HNO_3$ | $HF$ | $Cl^-$ | $Al^{3+}$ | $Hg^{2+}$ | $Ni^{2+}$ | $Cr_2O_7^{2-}$ | $Fe^{3+}$ | $Zr^{4+}$ | *25°C* | *95°C* |
| 3 | - | - | - | - | - | - | - | - | 0.006 | 0.052 |
| 3 | 0.05 | - | - | - | - | - | - | - | 0.44 | 12.8 |
| 3 | 0.05 | - | 0.05 | - | - | - | - | - | 0.28 | 6.3 |
| | 0.05 | - | 0.20 | - | - | - | - | - | 0.10 | 2.7 |
| | - | 0.06 | - | - | - | - | - | - | 0.04 | 0.11 |
| | - | 0.06 | - | 0.06 | - | - | - | - | 0.0002 | 0.22 |
| | - | 0.06 | - | 0.24 | - | - | - | - | 0.0006 | 0.0021 |
| | - | - | - | - | 0.005 | 0.005 | 0.04 | - | 0.053 | 5.0 |
| 7 | - | - | - | - | - | - | - | - | 0.008 | 0.17 |
| 7 | 0.05 | - | - | - | - | - | - | - | 7.0 | 20.5 |
| 7 | 0.05 | - | - | - | - | - | - | 0.05 | 0.006 | 0.30 |
| 7 | 0.05 | - | - | - | - | - | - | 0.20 | 0.003 | 0.13 |
| 7 | - | 0.06 | - | - | - | - | - | - | 0.008 | 6.2† |
| | - | 0.06 | - | 0.06 | - | - | - | - | 0.013 | 0.13 |
| | - | 0.06 | - | 0.24 | - | - | - | - | 0.007 | 0.13 |
| | - | - | - | - | 0.005 | 0.005 | 0.04 | - | 0.63 | 7.8 |

* Solutions changed once or twice a week.

** Corrosion is measured by weight loss rather than penetration because attack is nonuniform and primarily intergranular. Original weight of specimens: 170 to 200 grams.

† Soluble slag inclusion in weld.

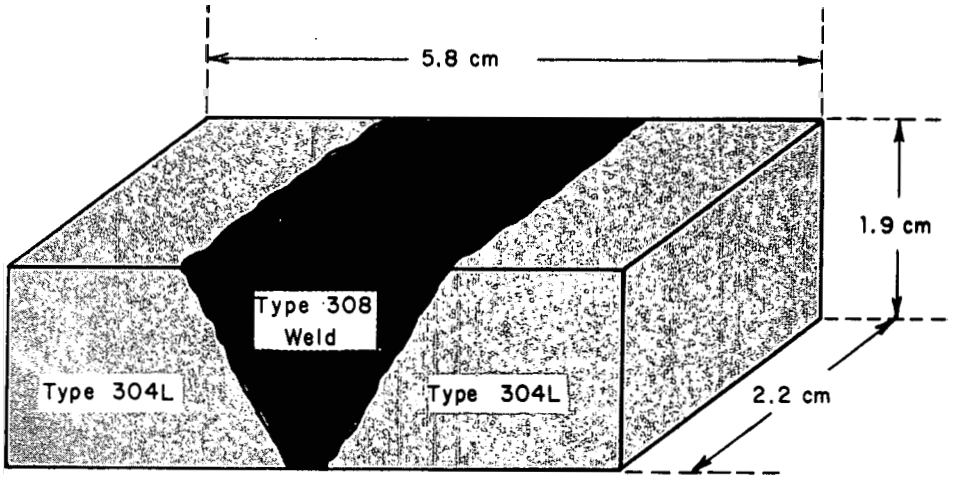


FIGURE 18. Typical Test Specimen of Type 304L Stainless Steel Welded with Type 308 Stainless Steel

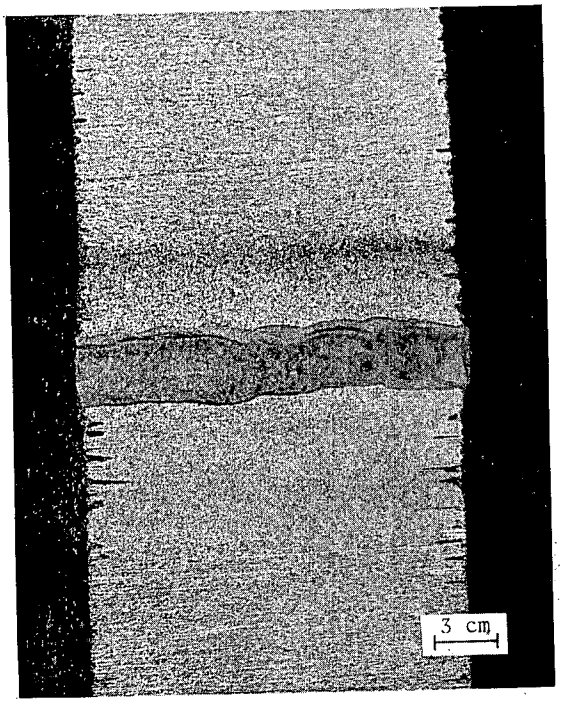


a. Attack in Heat-Affected Zone

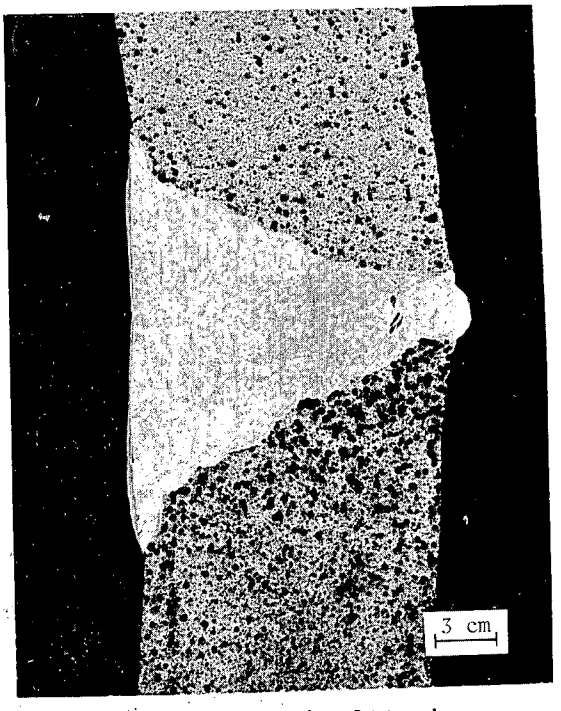


b. End-Grain Attack

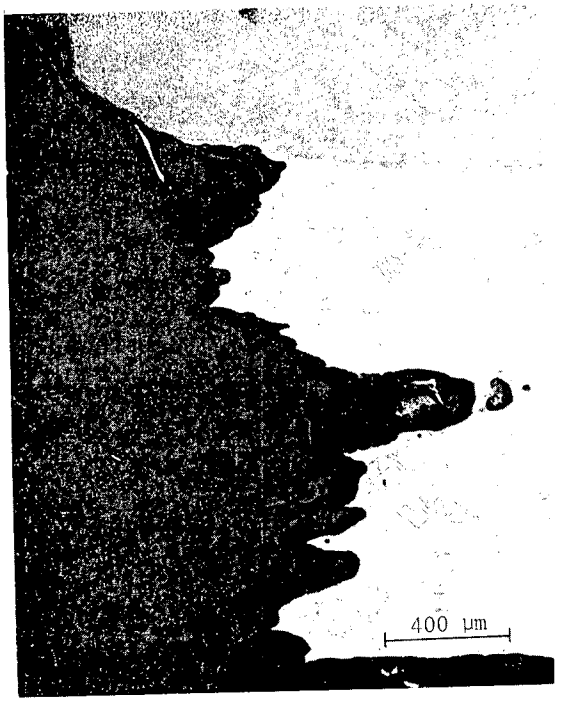


c. Attack Parallel to Rolling Direction. Note Deep Pits.


d. Perpendicular to Rolling Direction

FIGURE 19. Corrosion of Welded Type 304L Stainless Steel by 7M $HNO_3$ 0.05M HF at 95°C

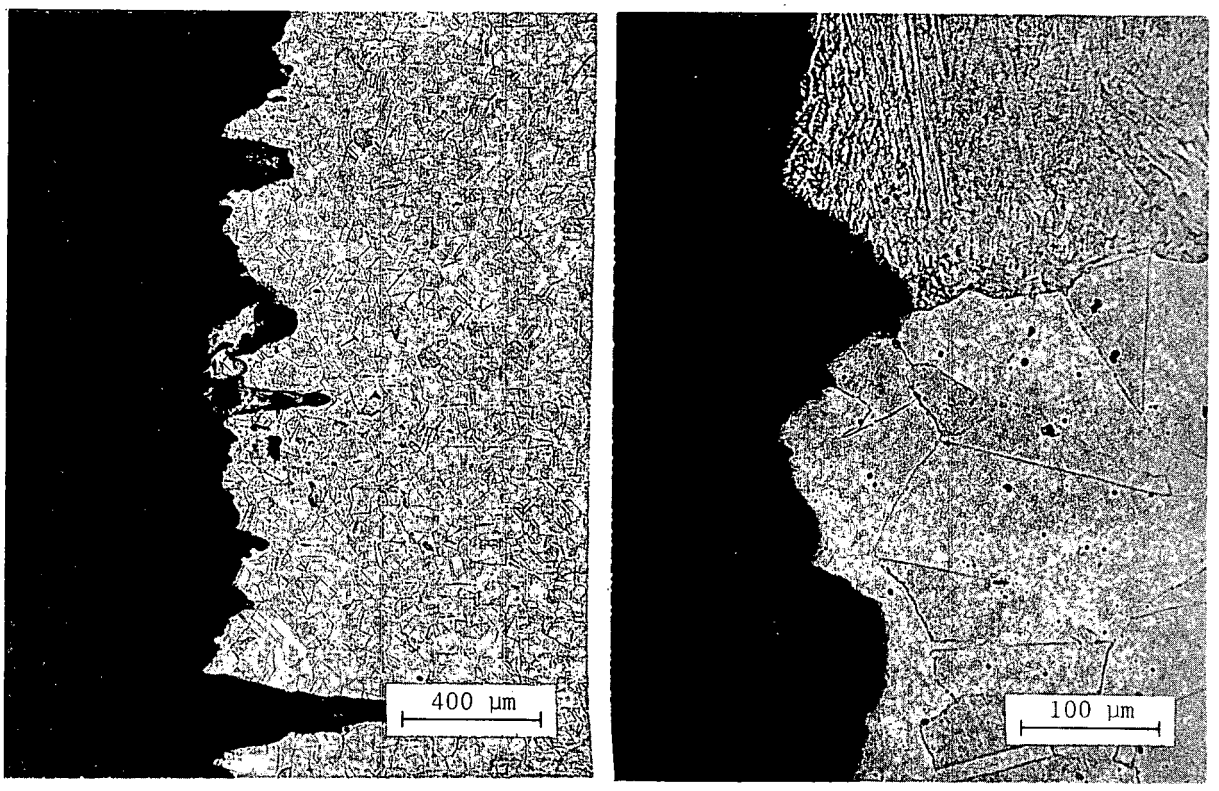


a. Pitting of End Grain

b. Attack Perpendicular to Rolling Direction

FIGURE 20. Corrosion of Welded Type 304L Stainless Steel in 3M $HNO_3$ - 0.05M HF at 95°C

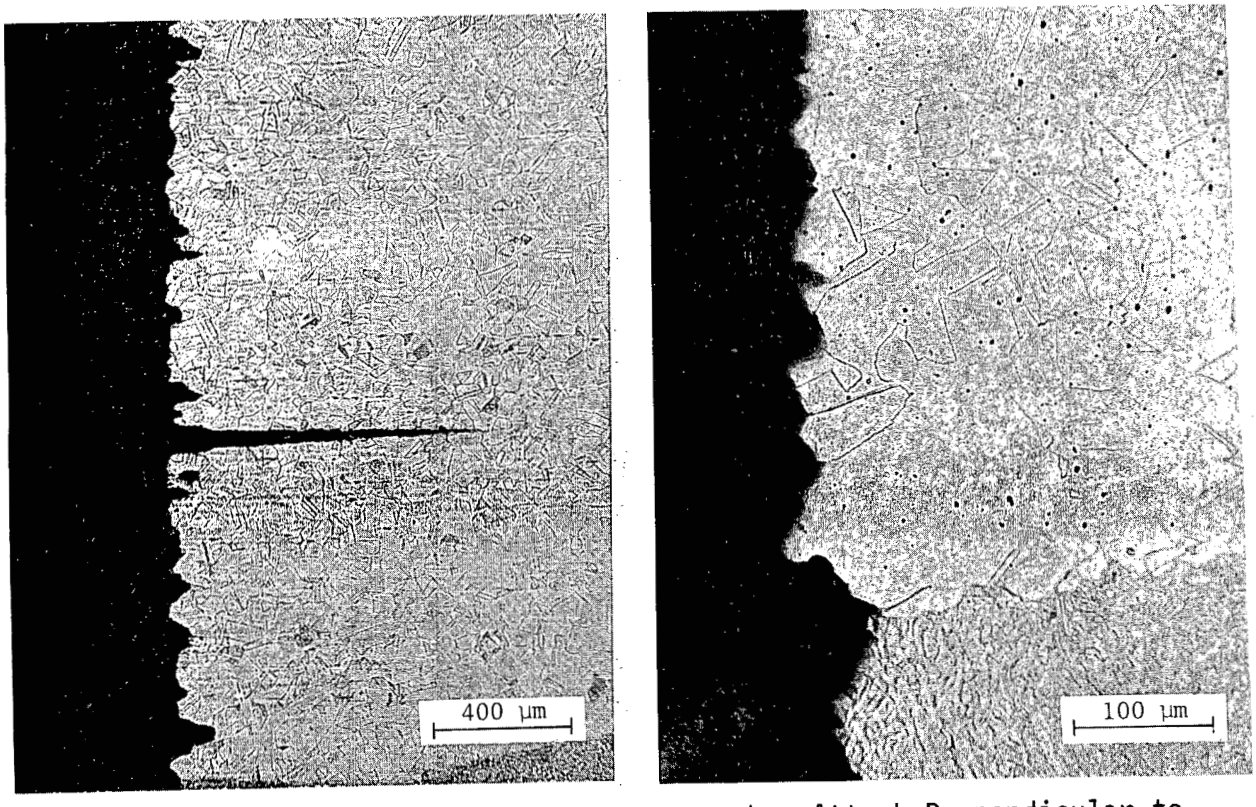


a. Pitting of End Grain

b. Attack Perpendicular to Rolling Direction

FIGURE 21. Corrosion of Welded Type 304L Stainless Steel in 3M $HNO_3$ - 0.05M HF - 0.20M Al at 95°C

TABLE 8

Weight Losses of Type 304L Stainless Steel

| *Test Solution* | *Relative Weight Loss* |
|---|---|
| 3M $HNO_3$ | 1.0 |
| 7M $HNO_3$ | 3.3 |
| 3M $HNO_3$ + 0.05M HF | 248 |
| 7M $HNO_3$ + 0.05M HF | 398 |
| 3M $HNO_3$ + 0.05M HF + 0.20M $Al(NO_3)_3$ | 52 |

Attack by $HNO_3$-Corrosion Products. Corrosion products, specifically $Fe^{3+}$ and $Cr_2O_7^{2-}$, are second to uncomplexed $F^-$ in aggressiveness because they increase intergranular attack autocatalytically. Since there are no complexing agents for $Cr_2O_7^{2-}$, corrosion of Type 304L stainless steel equipment should be minimized by use of complexing agents for $F^-$. Attack by $Cr_2O_7^{2-}$ is expected to be accelerated at higher temperatures and higher concentrations of $F^-$ and $HNO_3$. Equipment expected to be attacked includes waste evaporators, waste tanks (if operated at higher temperatures), and dissolvers (if the $F^-$ is not complexed). Off-gas systems for this equipment might also be attacked.

Attack by $HNO_3$-Chloride. As much as 2000 ppm (0.06M) chloride impurity in 3M to 7M $HNO_3$ had little effect on corrosion of Type 304L stainless steel because of the large excess of $NO_3^-$ ions occupying attack sites. Reduced corrosion due to complexing $Cl^-$ with $Hg^{2+}$ was observed in 3M $HNO_3$ but not in 7M $HNO_3$.

## Stress Corrosion Tests of Wedge-Opening-Loaded Specimens

Wedge-opening-loaded specimens[15] were exposed to various solutions that were expected to attack Type 304L stainless steel to see if cracks would propagate. Wedge-opening-loaded specimens are precracked blocks of steel that are loaded to a predetermined stress intensity at the tip of the crack (Figure 22). The sample is then exposed to a test solution, and the rate of crack extension is measured.

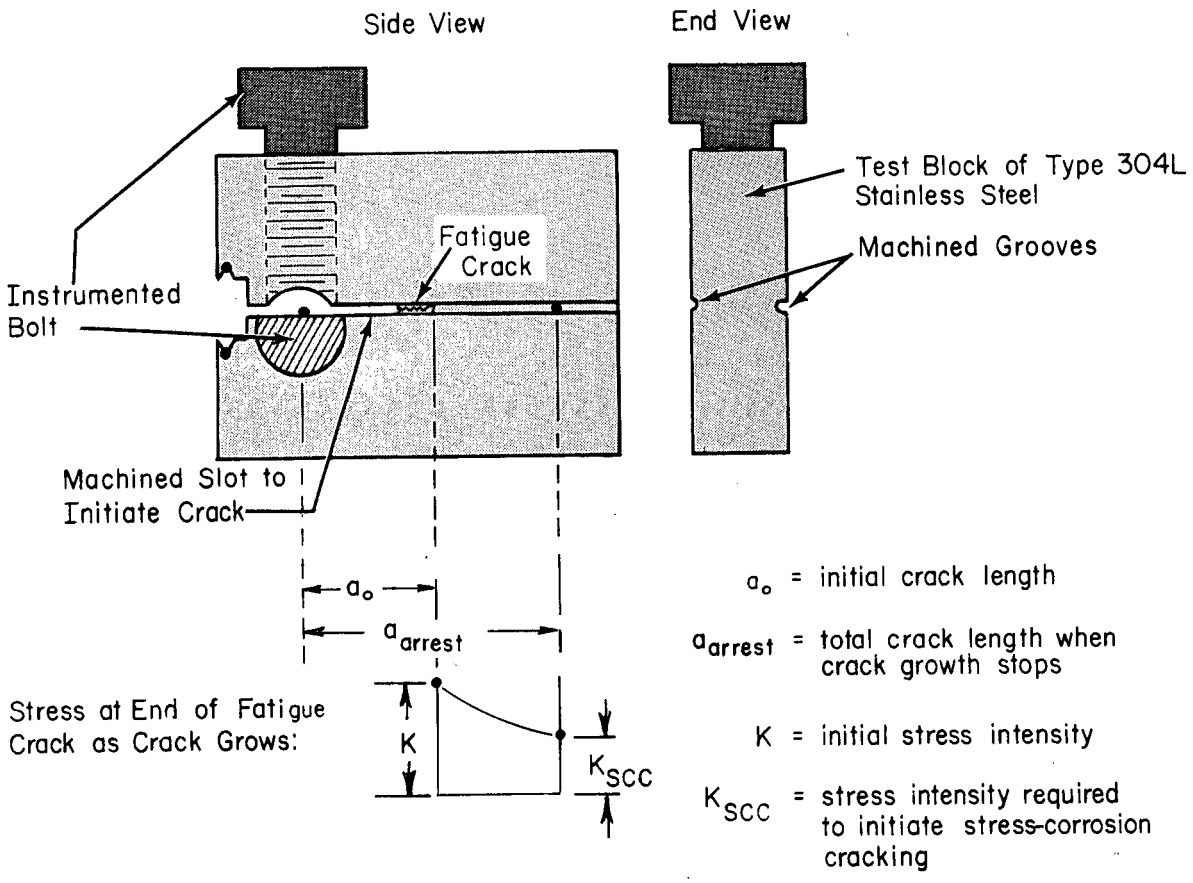


FIGURE 22. Wedge-Opening-Loaded Specimen of Type 304L Stainless Steel

As shown in Table 9, stainless steel specimens exposed to $MgCl_2$, a very aggressive solution used to evaluate cracking susceptibility, cracked rapidly. No cracking was observed in specimens exposed to other solutions. Except for one solution, some degree of intergranular attack occurred. Duplicate specimens exposed at 30°C (compared to 95°C for the other tests listed in Table 9) in waste from the first extraction bank (1AW) reprocessing Robinson $UO_2$ fuel did not show any attack after 2 years.

TABLE 9

Crack Propagation in Wedge-Opening-Loaded Specimens* of Type 304L Stainless Steel

| *Solution Composition* | *Exposure Temp., °C* | *Time, days* | *Observed Corrosion* |
|---|---|---|---|
| 45 wt % $MgCl_2$ | 95 | 2 | 0.47-inch crack |
| 7M $HNO_3$, 0.01M $CrO_4^{2-}$, 0.04M $Fe^{3+}$, 0.005M $Ni^{2+}$ | 95 | 58 | Severe intergranular |
| 7M $HNO_3$, 0.05M HF, 0.15M $Al^{3+}$ | 95 | 126 | Intergranular |
| 2M $HNO_3$, 0.05M HF, 0.05M $Cd^{2+}$ | 95 | 167 | Intergranular |
| 2M $HNO_3$, 0.06M NaCl | 95 | 195 | Light intergranular |
| 2M $HNO_3$ | 95 | 210 | Very light intergranular |
| HAW Waste from $UO_2$ Fuel | 30 | 180 | None |

*Specimens loaded to produce yielding at crack tip (39 kpsi$\sqrt{\text{inch}}$).

## REFERENCES


1. C. L. Peterson, et al. Construction Materials for Various Head-End Processes for the Aqueous Reprocessing of Spent Fuel Elements. USAEC Report BMI 1375, Battelle Memorial Institute, Columbus, OH (1969).

2. P. M. Kranzlein. Corrosion of Stainless Steel in $HNO_3$-HF Solutions. USAEC Report DP-486, E. I. du Pont de Nemours & Co. (Inc.), Savannah River Laboratory, Aiken, SC (1960).

3. J. L. English. Thorex Plant Corrosion Studies II. Corrosion of Types 304L, 309 SCb and 347 Stainless Steels During Development and Production-Development Periods. USAEC Report ORNL-2844, Oak Ridge National Laboratory, Oak Ridge, TN (1960).

4. R. F. Manness. Corrosion Evaluation of Nickel-Base Alloys Developed to Contain Power Reactor Fuel Dissolvents. USAEC Report HW-68426, Hanford Atomic Products, Richland, WA (1961).

5. C. S. Schlea and J. T. Lowe. Fluoride Complexing of U(VI) and Pu(IV) in Solutions Containing Al(III) and Zr(IV). USAEC Report DP-842, E. I. du Pont de Nemours & Co. (Inc.), Savannah River Laboratory, Aiken, SC (1964).

6. P. D. Miller, et al. Corrosion of Construction Materials in Boiling 13M Nitric-0.1M Hydrofluoric Acids. USAEC Report BMI-X-434, Battelle Memorial Institute, Columbus, OH (1967).

7. H. S. Cole. Corrosion of Austenitic Stainless Steel Alloys Due to $HNO_3$-HF Mixtures. USAEC Report ICP-1036, Idaho National Engineering Laboratory, Idaho Falls, ID (1974).

8. W. D. Clark and R. E. Blanco. Dissolution of LMFBR Fuels: Survey of the Corrosion of Selected Alloys in $HNO_3$-HF Solutions. USAEC Report ORNL-4745, Oak Ridge National Laboratory, Oak Ridge, TN (1971).

9. M. Stern and A. L. Geary. "Electrochemical Polarization: A Theoretical Analysis of the Shape of Polarization Curves." J. Electrochem. Soc. 104, 56 (1957).

10. P. E. Morris and R. C. Scarberry. "Predicting Corrosion Rates with a Potentiostat." Corrosion 24, 444 (1972).

11. L. G. Sillen, Complier. Stability Constants of Metal-Ion Complexes. Special Publication No. 17, The Chemical Society, London (1964).

12. M. L. Hyder, W. E. Prout, and E. R. Russell. Dissolution of Thorium Oxides. USAEC Report DP-1044, E. I. du Pont de Nemours & Co. (Inc.), Savannah River Laboratory, Aiken, SC (1966).

13. J. W. Diggle, Ed. Oxides and Oxide Films. Vol I, p 239, Marcel Dekker, Inc., New York (1972).

14. R. S. Ondrejcin. "A Stress Corrosion Cracking Test with Slow Strain Rate and Constant Current." Stress Corrosion Cracking - The Slow Strain Rate Techniques. Special Technical Publication 655, American Society for Testing of Materials, Philadelphia, PA (1979).

15. S. R. Novak and S. T. Rolfe. "Modified WOL Specimen for $K_{ISCC}$ Environmental Testing." J. Mat. 4, 701 (1969).